STATE OF CALIFORNIA • DEPARTMENT OF TRANSPORTATION

# TECHNICAL REPORT DOCUMENTATION PAGE

TR-0003 (REV 04/2024)

| 1. REPORT NUMBER | 2. GOVERNMENT ASSOCIATION NUMBER | 3. RECIPIENT'S CATALOG NUMBER |
|---|---|---|
| CA26-4051 | | |

| 4. TITLE AND SUBTITLE | 5. REPORT DATE |
|---|---|
| Behavior in Vegetative Barriers of Aerosol Particulate Matter2.5 (PM2.5) and PM10 along Highways | May 2026 |
| | 6. PERFORMING ORGANIZATION CODE<br>N/A |

| 7. AUTHOR | 8. PERFORMING ORGANIZATION REPORT NO. |
|---|---|
| Loralee Larios, Akula Venkatram | N/A |

| 9. PERFORMING ORGANIZATION NAME AND ADDRESS | 10. WORK UNIT NUMBER |
|---|---|
| Department of Mechanical Engineering<br>Bourns Hall A342<br>900 University Ave.<br>University of California, Riverside<br>Riverside, CA 92521 | N/A |
| | 11. CONTRACT OR GRANT NUMBER<br>65A1022 |

| 12. SPONSORING AGENCY AND ADDRESS | 13. TYPE OF REPORT AND PERIOD COVERED |
|---|---|
| California Department of Transportation (Caltrans)<br>Division of Research, Innovation and System Information, MS-83<br>1727 30th Street Sacramento, CA 95816 | Final Report |
| | 14. SPONSORING AGENCY CODE<br>N/A |

15. SUPPLEMENTARY NOTES

NA

16. ABSTRACT

There is consensus on elevated health risks for populations living, working, or going to school near roadways. Options to mitigate the impacts of traffic emissions include roadside solid and vegetative barriers, which increase vertical dispersion of emissions and hence reduce concentrations of highway pollutants next to roadways. While roadside vegetation barriers have shown the potential to reduce near-road air pollution concentrations, the characteristics of these barriers needed to ensure pollution reductions are not well understood. The primary objective of the project was to create a modeling tool that can simulate scenarios and recommend optimal vegetative barriers for California's transportation network. This tool, called the Vegetative Barrier Model (VBM), simulates the impact of roadside barriers, with and without vegetation, on the concentrations of vehicle-related particulate matters (PM2.5 and PM10) and provides quantitative information for planning of vegetative barriers to reduce air pollution and advance equity and livability in communities located near roads. The primary data set that was used in the formulation and evaluation of VBM consisted of measurements made during 2024-2025 at a location on SR-55 on Orange County, Southern California, which consisted of a stretch of highway that included a solid barrier, and vegetative barrier, and an open section. This unique configuration allowed us to compare the impact of three types of barriers on near-road air quality. VBM is based on the idea that the impact of a vegetative barrier can be modeled as an interpolation between concentration estimates from the well-established solid barrier model and those from a section with no-barrier. The porosity of the vegetation is used to interpolate between these two estimates. We formulated a method to use measurements from the SR-55 site to evaluate this concept underlying VBM. Data from a field study conducted in Woodside, California, in 2014 next to I-280 was used to evaluate the model. VBM consists of two sub-models: a Dispersion Model (DM) and a Volatile Organic Compounds Emission Model (VEM). The DM estimates particulate matter concentrations at specified receptors, while the VEM estimates emission rates of biogenic volatile organic compounds from the specified vegetative barrier. DM and the VEM are currently coded in MATLAB. These sub-models are packaged in an executable VBM with an interface that facilitates its application by a non-expert.

| 17. KEY WORDS | 18. DISTRIBUTION STATEMENT |
|---|---|
| Vegetative barrier, solid barrier, barrier model, particulate matter, PM, PM2.5, PM10, | |

| 19. SECURITY CLASSIFICATION *(of this report)* | 20. NUMBER OF PAGES | 21. COST OF REPORT CHARGED |
|---|---|---|
| Unclassified | 93 | |

# *Behavior in Vegetative Barriers of Aerosol Particulate Matter ($PM_{2.5}$ and $PM_{10}$) along Highways*

**Prepared for**

**California Department of Transportation**

**Caltrans Contract # 65A1022**

**March 2025**


**Principal Investigators:**

**Loralee Larios,**

**Akula Venkatram**

**Department of Mechanical Engineering**

**University of California, Riverside**

**Riverside, CA 92521**

**(951) 827-2105**



# DISCLAIMER

This document is disseminated in the interest of information exchange. The contents of this report reflect the views of the authors who are responsible for the facts and accuracy of the data presented here. The contents do not necessarily reflect the official views or policies of the State of California. This publication does not constitute a standard, specification, or regulation. This report does not constitute an endorsement by the California Department of Transportation of any product described in this report.

# ACKNOWLDEDGEMENTS

We thank the following organizations and individuals for their time, effort, and resources in contributing to the success of this project. The field measurements were made possible through the support of many people whose contributions we gratefully acknowledge. Dr. Amir Saeidi assisted in designing the field studies, led the team of UCR graduate and undergraduate students who conducted them, and played a major role in analyzing the data. We also thank undergraduate students Olivia Halseth, Maisha Gupta, and Yusuf Jameel for their commitment to learning new tasks, working effectively as a team, and contributing long hours in the field.

We are grateful to the California Department of Transportation (Caltrans) for their support of the work described in this report. In particular, we thank Dr. Simon Bisrat and Daisy Laurino for their guidance on both technical and administrative aspects of the project. We also appreciate the scientists from the California Air Resources Board and the U.S. Environmental Protection Agency who served on our Project Advisory Committee and provided constructive feedback throughout the project.

# EXECUTIVE SUMMARY

There is consensus on elevated health risks for populations living, working, or going to school near large roadways. The health concerns have been linked to elevated levels of air pollution caused by traffic emissions (see HEI, 2010). Options to mitigate the impacts of traffic emissions include roadside solid and vegetative barriers (Baldauf et al., 2009), which increase vertical dispersion of emissions and hence reduce concentrations of highway pollutants next to roadways. Roadside barriers have other positive effects. Solid roadside barriers, already present at many highways, reduce the transmission of noise from highway vehicles to near-road environments. Vegetative barriers can reduce visual awareness of traffic resulting in a general perception of lower noise levels, and also enhance highway aesthetics. While roadside vegetation barriers have shown the potential to reduce near-road air pollution concentrations, the characteristics of these barriers needed to ensure pollution reductions are not well understood. The project described in this report is designed to address the uncertainty associated with the impact of vegetative barriers.

The primary objective of the project is to create a modeling tool that can simulate scenarios and recommend optimal vegetative barriers for California's transportation network that protects all near road communities from air pollutants. This tool, called the Vegetative Barrier Model (VBM), simulates the impact of roadside barriers, with and without vegetation, on the concentrations of vehicle-related PM2.5/PM10 in the near-road environment, which is the order of a kilometer from the road. It provides quantitative information for planning of vegetative barriers to reduce air pollution and advance equity and livability in communities located near roads.

The project was conducted over a period of 35 months from the start of the project. Fulfilling the research objective addressed the following major tasks: 1) Compiling the data base required to develop and evaluate the model, 2) Developing methods to relate properties of vegetation to variables required by VBM, and 3) Developing a model to estimate resuspended PM10 and PM2.5 using readily available inputs.

Our examination of field studies relevant to objectives of this project allowed us to select two field studies for data that could be used for the development of VBM. The first field study, conducted in Woodside, California, in 2014 next to I-280 (Deshmukh et al., 2019). The second field study was conducted by UCR in 2016 in Sacramento, California, on the impact of a barrier with tall vegetation behind it in mitigating the impact of vehicle emissions (Ahangar et al., 2017). The

Woodside data was used in the evaluation of VBM, while that from Sacramento provided qualitative guidance on the formulation of VBM.

The primary data set that was used in the formulation and evaluation of VBM consisted of measurements made during 2024-2025 at a location on SR-55 on Orange County, Southern California, which consisted of a stretch of highway that included a solid barrier, and vegetative barrier, and an open section. This unique configuration allowed us to compare the impact of three types of barriers on near-road air quality. Because the background concentrations of particulate matter were high relative to the contribution from the highway, the measuring instrumentation did not allow us to make simultaneous measurements at the three locations using different sensors with precision errors comparable to the particulate contributions from the highways. It was necessary to develop and implement a measurement strategy that relied on making measurements with a mobile platform instrumented with a single PurpleAir monitor; this allowed us to avoid errors associated with the precision of different sensors. The PM measurements were accompanied with meteorological measurements with a 3-D sonic anemometer located upwind of the site.

The field study included measurements of the characteristics of vegetative barriers at the SR-55 site and other locations in Southern California with vegetative roadside barriers. The characteristics included optical porosity, Leaf Area Index, species of the vegetation and dimensions of barriers, which are used in VBM to estimate deposition and volatile organic emissions from barriers.

The Vegetative Barrier Model (VBM) is based on the idea that the impact of a vegetative barrier can be modeled as an interpolation between concentration estimates from the well-established solid barrier model and those from a section with no-barrier. The porosity of the vegetation is used to interpolate between these two estimates. We formulated a method to use measurements from the SR-55 site to evaluate this concept underlying VBM. This evaluation is supported by data from the site in Woodside, California.

The Vegetative Barrier Model consists of two sub-models: Dispersion Model (DM), and VOC Emission Model (VEM). The DM estimates particulate matter concentrations at specified receptors, while the VEM estimates emission rates of biogenic volatile organic compounds from the specified vegetative barrier. The VEM is based on the MEGAN model (*Model of Emissions of Gases and Aerosols from Nature;* Guenther et al. ;2012). DM and the VEM are currently coded

in MATLAB. These sub-models are packaged in an executable VBM with an interface that facilitates its application by a non-expert.

## Table of Contents

## Table of Figures

## Table of Tables

# Chapter 1

## Objectives of Project, Tasks, and Schedule

## 1.1 Motivation

There is broad consensus that populations living, working, or attending school near major roadways face elevated health risks. These risks are largely attributed to increased exposure to traffic-related air pollutants (see HEI, 2010). As a result, there has been growing interest in strategies to mitigate the impacts of roadway emissions on nearby communities.

Traditionally, transportation and land-use planning approaches have focused on reducing emissions at the source through stricter vehicle emission standards and decreased vehicle activity, as well as on implementing buffer or exclusion zones. However, these measures are typically long-term solutions, as they require regulatory changes, infrastructure planning, and sustained reductions in vehicle miles traveled.

More immediate mitigation strategies emphasize roadway design and urban planning interventions, including road placement and configuration, as well as the use of roadside solid barriers and vegetation (Baldauf et al., 2009). Among these, roadside barriers offer a particularly attractive option because they can be implemented relatively quickly and at comparatively low cost. In many cases, such barriers are already in place for noise reduction and may also provide ancillary benefits by lowering near-road pollutant exposures. Additionally, roadside barriers can enhance the visual aesthetics of transportation corridors.

Despite the numerous real-world measurements that have been devoted to examine the effect of vegetative barriers on air quality near roadways, conclusions on their effects are not definitive. Al-Dabbous and Kumar (2014) measured concentrations of particles within the size range of 5 – 560 nm in the vicinity of a roadway in Guildford, Surrey, UK. They observed that the concentration right behind the 2.2 m thick vegetation barrier was 37% smaller than the concentration measured right next to the roadway at a clearing section. Because the receptor behind vegetation was 2.2 m further from the roadway than the receptor at the clear section, the actual reduction due to the

presence of a vegetative barrier is probably less than the reported value. A field study was done in Finland by deploying passive and active samplers (Setala et al., 2013) under tree-canopies in tree-covered park areas and in adjacent treeless areas in the vicinity of twenty sites in Helsinki and Lahti. Passive samplers showed insignificant decreases of $NO_2$, 19% reduction of VOC, and 35 – 40% reduction of the mass deposited. However, active samplers showed 20% reduction of fine particles (20 – 1000 nm), and no difference for $PM_{2.5}$ and $PM_{10}$ particles. Field studies conducted on evergreen and deciduous trees in North Carolina, USA (Hagler et al., 2012) also concluded that vegetation can lead to higher, lower, or the same level of concentration as the clearing section. Another field study conducted in Detroit, Michigan (Brantley et al., 2014) showed that the presence of 15 m thick vegetation barrier results in 12% reduction in black carbon concentrations, while it does not change the particle counts in the fine and coarse particle size range (0.5 – 1.0 $\mu m$ aerodynamic diameter). A field campaign conducted in Queens, New York City (Tong et al., 2015) indicated higher concentrations behind the vegetation barrier presumably because of decreased values of Turbulent Kinetic Energy (TKE) behind the vegetative barrier.

Several modeling and wind-tunnel studies have been conducted to describe the effects of vegetative barriers on urban air pollution. Steffens et al. (2012) incorporated particle aerodynamics and deposition mechanisms into the Comprehensive Turbulent Aerosol Dynamics and Gas Chemistry (CTAG) model to examine the effects of vegetative barriers on roadway-emitted pollutants. They modeled the results of the field experiment conducted in Chapel Hill, NC (Hagler et al., 2012). They assumed that vegetative barriers affect near-road air quality in the following ways: 1) particles are deposited on leaf surfaces, 2) downwind wind speed and turbulence levels in the flow passing through the barrier are decreased, and 3) a fraction of the flow carrying pollutants is forced to go over the barrier. The first and third effects mitigate air pollution, while the second effect leads to higher concentrations. Another Computation Fluid Dynamics model developed by (Vos et al., 2013) found that concentrations within street canyons are higher when trees are present. They found that the effect of vegetation decreasing turbulent kinetic energy (TKE) is stronger than its filtration capacity, thus vegetation increases local concentrations within street canyons. Wind tunnel studies conducted on the effects of trees within street canyons showed that trees increase concentrations at the leeward wall and decrease concentrations only slightly on the windward side (Gromke and Ruck, 2012).

So far, only a few studies have been performed which explicitly investigate the effects of a combination of vegetation and solid barrier on the air quality near roadways. Baldauf et al. (2008) conducted a comprehensive field study in Raleigh, NC where a stretch of a clearing, a solid barrier, and a vegetation-solid barrier combination was present. The results indicated that concentrations measured next to solid-vegetation barrier mitigated downwind concentrations more than either the solid barrier or the vegetative barrier by themselves. Similar measurements made in Sacramento, California,(Enayati Ahangar et al., 2017) indicate that tall vegetation planted behind a solid barrier reduces the entrainment of pollutants into the cavity downwind of the solid barrier, thus enhancing the mitigating impact of the solid barrier. A Computational Fluid Dynamics (CFD) model based on Large Eddy Simulation (LES) examined the effects of common vegetative barrier configurations near roadways to find the most effective configuration (Tong et al., 2016). The results indicated that a wide vegetation barrier with high Leaf Area Density (LAD), and also a combination of vegetation and solid barrier work best as mitigation strategies.

There is a need to conduct experiments that provide more conclusive results, and develop models, based on results from the experiments, which allow estimation of the effects of vegetative barriers. This report summarizes the results of project, funded by Caltrans, to satisfy this need.

## 1.2 Objectives of Project and Task Structure

The primary objective of this project is to create a modeling tool that can simulate scenarios and recommend optimal vegetative barriers for California's transportation network that protects all near road communities from air pollutants. This tool, which will be called the Vegetative Barrier Model (VBM), will simulate the impact of roadside barriers, with and without vegetation, on the concentrations of vehicle-related PM2.5/PM10 in the near-road environment. It will provide quantitative information for planning of vegetative barriers to reduce air pollution and advance equity and livability in underserved communities located near roads.

**Task 1: Compile a database required to develop VBM (UCR will manage this database until it is delivered to Caltrans)**

**Task 2: Formulate Model (VBM)**

**Task 3: Conduct field studies to collect data required to evaluate modeling tool**

**Task 4: Evaluate modeling tool**

**<u>Task 5</u>: Provide Online Training**

## 1.3 Schedule

*Period of Performance:* The project was initiated on February 1, 2023, and completed in 35 months from the start date.

*Tasks and Schedule:* Project Schedule is given below.

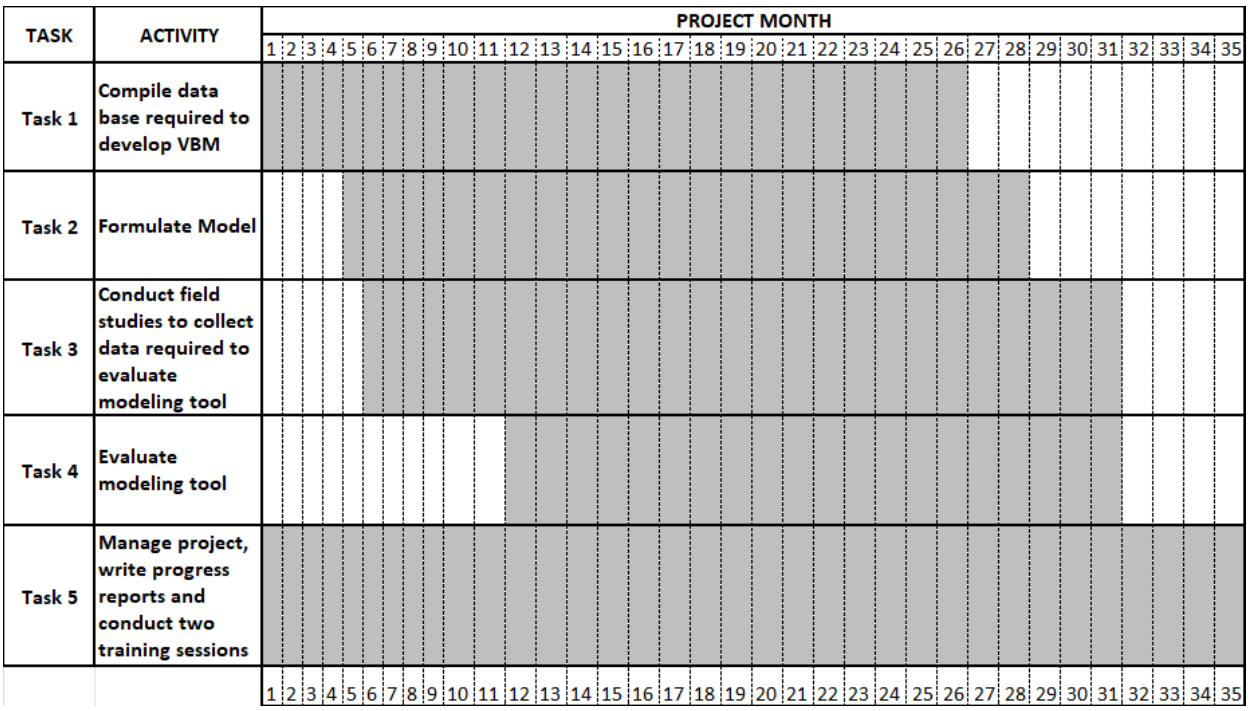


**Figure 1.1.** *Schedule of the Project*

The following Chapters describe details of accomplishing Tasks 1 to 4.

## 1.4 References


- Ahangar, F., Amini, S., Venkatram, A., 2017. Using Vegetation to Enhance the Impact of Solid Barriers on Near-road Air Pollution, in: A&WMA's 110th Annual Conference & Exhibition. A&WMA's 110th Annual Conference & Exhibition, Pittsburgh.
- Ahangar, F.E., Heist, D., Perry, S., Venkatram, A., 2017. Reduction of air pollution levels downwind of a road with an upwind noise barrier. Atmos. Environ. doi:10.1016/j.atmosenv.2017.02.001
- Al-Dabbous, A.N., Kumar, P., 2014. The influence of roadside vegetation barriers on airborne nanoparticles and pedestrians exposure under varying wind conditions. Atmos. Environ. 90, 113–124.
- Amini, S., Ahangar, F.E., Schulte, N., Venkatram, A., 2016. Using models to interpret the impact of roadside barriers on near-road air quality. Atmos. Environ. 138, 55–64. https://doi.org/10.1016/j.atmosenv.2016.05.001
- Baldauf, R., Thoma, E., Khlystov, A., Isakov, V., Bowker, G., Long, T., Snow, R., 2008. Impacts of noise barriers on near-road air quality. Atmos. Environ. 42, 7502–7507.
- Bowker, G.E., Baldauf, R., Isakov, V., Khlystov, A., Petersen, W., 2007. The effects of roadside structures on the transport and dispersion of ultrafine particles from highways. Atmos. Environ. 41, 8128–8139.
- Brantley, H.L., Hagler, G.S.W., J. Deshmukh, P., Baldauf, R.W., 2014. Field assessment of the effects of roadside vegetation on near-road black carbon and particulate matter. Sci. Total Environ. 468–469, 120–129.
- Finn, D., Clawson, K.L., Carter, R.G., Rich, J.D., Eckman, R.M., Perry, S.G., Isakov, V., Heist, D.K., 2010. Tracer studies to characterize the effects of roadside noise barriers on near-road pollutant dispersion under varying atmospheric stability conditions. Atmos. Environ. 44, 204–214.
- Gromke, C., Ruck, B., 2012. Pollutant Concentrations in Street Canyons of Different Aspect Ratio with Avenues of Trees for Various Wind Directions. Boundary-Layer Meteorol. 144, 41–64. doi:10.1007/s10546-012-9703-z

- Guenther, A.B., Jiang, X., Heald, C.L., Sakulyanontvittaya, T., Duhl, T., Emmons, L.K., Wang, X., 2012. The model of emissions of gases and aerosols from nature version 2.1 (MEGAN2.1): An extended and updated framework for modeling biogenic emissions. Geosci. Model Dev. 5, 1471–1492. https://doi.org/10.5194/gmd-5-1471-2012
- Hagler, G.S.W., Lin, M.Y., Khlystov, A., Baldauf, R.W., Isakov, V., Faircloth, J., Jackson, L.E., 2012. Field investigation of roadside vegetative and structural barrier impact on near-road ultrafine particle concentrations under a variety of wind conditions. Sci. Total Environ. 419, 7–15.
- Hagler, G.S.W., Tang, W., Freeman, M.J., Heist, D.K., Perry, S.G., Vette, A.F., 2011. Model evaluation of roadside barrier impact on near-road air pollution. Atmos. Environ. 45, 2522–2530. doi:10.1016/j.atmosenv.2011.02.030
- Hagler, G.S.W., E.D. Thoma, R.W. Baldauf, 2010: High-Resolution Mobile Monitoring of Carbon Monoxide and Ultrafine Particle Concentrations in a Near-Road Environment, J. *Air & Waste Manage Assoc*. **60**, 328–336
- Heist, D.K., Perry, S.G., Brixey, L.A., 2009. A wind tunnel study of the effect of roadway configurations on the dispersion of traffic-related pollution. Atmos. Environ. 43, 5101–5111.
- Health Effects Institute (HEI). (2010). *Traffic-Related Air Pollution: A Critical Review of the Literature on Emissions, Exposure, and Health Effects*. HEI Special Report 17.
- Kenney, W.A., 1987. A method for estimating windbreak porosity using digitized photographic silhouettes. Agric. For. Meteorol. 39, 91–94. https://doi.org/10.1016/0168-1923(87)90028-1
- Kumar, P., Ketzel, M., Vardoulakis, S., Pirjola, L., Britter, R., 2011. Dynamics and dispersion modelling of nanoparticles from road traffic in the urban atmospheric environment-A review. J. Aerosol Sci. 42, 580–603.
- Schulte, N., Snyder, M., Isakov, V., Heist, D., Venkatram, A., 2014. Effects of solid barriers on dispersion of roadway emissions. Atmos. Environ. 97, 286–295. doi:10.1016/j.atmosenv.2014.08.026

- Schulte, N., Tan, S., Venkatram, A., 2015. The ratio of effective building height to street width governs dispersion of local vehicle emissions. Atmos. Environ. 112, 54–63. doi:10.1016/j.atmosenv.2015.03.061
- Setälä, H., Viippola, V., Rantalainen, A.-L., Pennanen, A., Yli-Pelkonen, V., 2013. Does urban vegetation mitigate air pollution in northern conditions? Environ. Pollut. 183, 104–12. doi:10.1016/j.envpol.2012.11.010
- Steffens, J.T., Wang, Y.J., Zhang, K.M., 2012. Exploration of effects of a vegetation barrier on particle size distributions in a near-road environment. Atmos. Environ. 50, 120–128.
- Tong, Z., Baldauf, R.W., Isakov, V., Deshmukh, P., Max Zhang, K., 2016. Roadside vegetation barrier designs to mitigate near-road air pollution impacts. Sci. Total Environ. 541, 920–7. doi:10.1016/j.scitotenv.2015.09.067
- Tong, Z., Whitlow, T.H., MacRae, P.F., Landers, A.J., Harada, Y., 2015. Quantifying the effect of vegetation on near-road air quality using brief campaigns. Environ. Pollut. 201, 141–149. doi:10.1016/j.envpol.2015.02.026
- Venkatram, A., Fitz, D., Bumiller, K., Du, S.M., Boeck, M., Ganguly, C., 1999. Using a dispersion model to estimate emission rates of particulate matter from paved roads. Atmos. Environ. 33, 1093–1102. https://doi.org/10.1016/S1352-2310(98)00316-1
- Venkatram, A., Isakov, V., Deshmukh, P., & Baldauf, R. (2016). Modeling the impact of solid noise barriers on near road air quality. *Atmospheric Environment*, *141*, 462-469.
- Vos, P.E.J., Maiheu, B., Vankerkom, J., Janssen, S., 2013. Improving local air quality in cities: To tree or not to tree? Environ. Pollut. 183, 113–122. doi:10.1016/j.envpol.2012.10.021
- Wang, H., Takle, E.S., 1995. A numerical simulation of boundary-layer flows near shelterbelts. Boundary-Layer Meteorol. 75, 141–173. doi:10.1007/BF00721047

# Chapter 2

## Compilation of Data Bases For Analysis

## 2.1 Introduction

Numerous real-world measurements that have been devoted to examining the effect of vegetative barriers on air quality near roadways. Al-Dabbous and Kumar (2014) measured concentrations of particles within the size range of 5 – 560 nm in the vicinity of a roadway in Guildford, Surrey, UK. They observed that the concentration right behind the 2.2 m thick vegetation barrier was 37% smaller than the concentration measured right next to the roadway at a clearing section. Because the receptor behind vegetation was 2.2 m further from the roadway than the receptor at the clear section, the actual reduction due to the presence of a vegetative barrier is probably less than the reported value.

A field study was conducted in Finland by deploying passive and active samplers (Setala et al., 2013) under tree-canopies in tree-covered park areas and in adjacent treeless areas in the vicinity of twenty sites in Helsinki and Lahti. Passive samplers showed insignificant decreases of $NO_2$, 19% reduction of VOC, and 35 – 40% reduction of the mass deposited. However, active samplers showed 20% reduction of fine particles (20 – 1000 nm), and no difference for $PM_{2.5}$ and $PM_{10}$ particles.

Field studies conducted on evergreen and deciduous trees in North Carolina, USA (Hagler et al., 2012) also concluded that vegetation can lead to higher, lower, or the same level of concentration as the clearing section. Another field study conducted in Detroit, Michigan (Brantley et al., 2014) showed that the presence of 15 m thick vegetation barrier results in 12% reduction in black carbon concentrations, while it does not change the particle counts in the fine and coarse particle size range (0.5 – 1.0 $\mu m$ aerodynamic diameter).

A field campaign conducted in Queens, New York City (Tong et al., 2015) indicated higher concentrations behind the vegetation barrier presumably because of decreased values of Turbulent Kinetic Energy (TKE) behind the vegetative barrier.

So far, only a few studies have been performed which explicitly investigate the effects of a vegetative barrier relative to the impact of solid barrier on the air quality near roadways. Baldauf et al. (2008) conducted a comprehensive field study in Raleigh, NC where a stretch of a clearing, a solid barrier, and a vegetation-solid barrier combination was present. The results indicated that concentrations measured next to the solid-vegetation barrier mitigated downwind concentrations more than the other two barriers individually.

Our examination of field studies relevant to the objectives of this project allowed us to select two field studies for data that could be used for the development of VBM. The first field study, conducted in Woodside, California, in 2014 next to I-280 (Deshmukh et al., 2019). The second field study was conducted by UCR in 2016 in Sacramento, California, on the impact of a barrier with tall vegetation behind it in mitigating the impact of vehicle emissions (Ahangar et al., 2017). Each of these studies is described in the following sections.

## 2.2 Woodside Field Study

The field study consisted of air quality measurements during the summer season in Woodside, California, USA near a highway with vegetation planted along the roadside. Details of the study are described in Deshmukh et al., (2019). Only the relevant information is covered here.

The field study location, illustrated in Figure 2.1, included a segment of open area with no obstructions to air flow and a long segment of roadside vegetation along the same stretch of limited-access highway (Interstate-280). This highway supported approximately 125,000 vehicles per day during the study. An access road parallel to the highway and behind the vegetation had less than 200 vehicles per day during the study. Figure 2.1 shows an aerial view of the site. As shown at the bottom of Figure 2.1, six locations (labeled “Stops”) were identified with differing vegetation characteristics. Table 2.1 lists the Stop numbers, descriptors, and details on the vegetation characteristics corresponding to the locations shown in Figure 2.1.

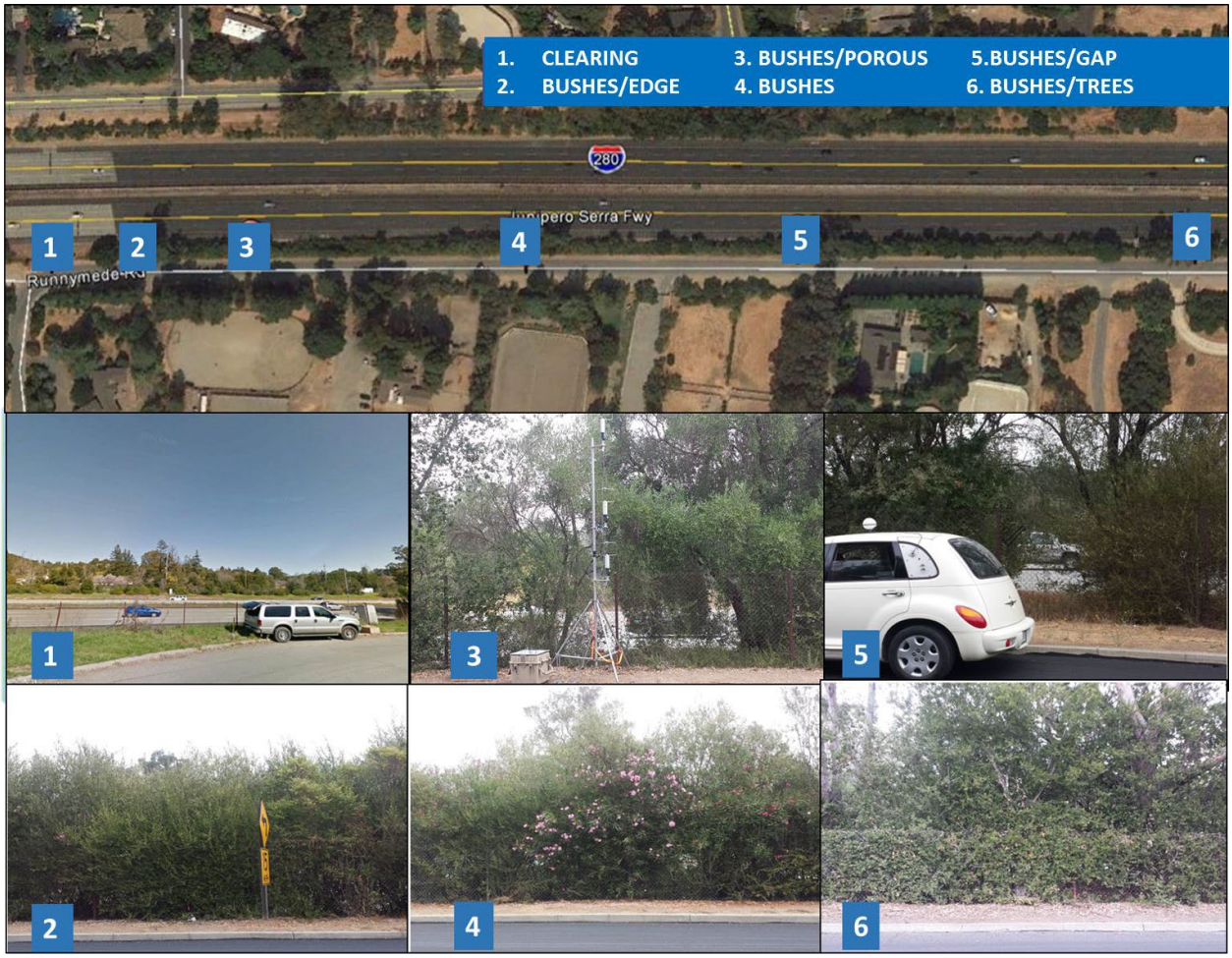


**Figure 2.1.** *Aerial view of the study location including Interstate-280, the parallel access road, and the neighborhood to the south of the highway. The inserts at the bottom show a view of the vegetation characteristics at each measurement location, which correspond to the estimates of vegetation porosity at each location as listed in Table 2.1.*

**Table 2.1.** *Characteristics of Sites Sampled at Woodside, California*

| Stop | Descriptor | Height(m) | Width(m) | Porosity* | Notes |
|---|---|---|---|---|---|
| **1** | CLEARING | <1 | <1 | 100 | Grass and low bushes only; no obstruction to air flow |
| **2** | BUSHES/EDGE | 3 | 5 | 25 | Bushes only; located approximately 20m from clearing |
| **3** | BUSHES/POROUS | 5 | 5 | 50 | Porous vegetation with bushes and trees, including large gaps with limited or no vegetation |
| **4** | BUSHES | 4 | 10 | 10 | Mix of thick bushes and flowering oleanders |
| **5** | BUSHES/GAP | 5 | 10 | 25/90 | Bushes (25% porosity) on either side of an approximately 1.5m wide, gap (90% porosity) |
| **6** | BUSHES/TREES | 10 | 10 | 10 | Mix of bushes approximately 2m tall with trees extending above to approximately 10m |

* Porosity estimated visually from pictures as shown in Figure 2.1.

As described in Table 2.1, Stop 1 (CLEARING) was an open area with the vegetation consisting of only low grass and isolated bushes less than 1 meter in height and width and no other major obstructions to air flow. The vegetative barrier beyond Stop 1 consisted of a mixture of planted hedges and oleander bushes with scattered trees growing among the bushes. The porosity of the vegetation varied along the study area. The majority of the vegetation had low porosity, as shown for Stops 2 (BUSHES/EDGE), 4 (BUSHES) and 6 (BUSHES/TREES) in Figure 2.1; however, two locations, Stops 3 (BUSHES/POROUS) and 5 (BUSHES/GAP) had large spacing within and between the bushes, where the vegetation either grew sporadically or did not grow at all. The porosities in Table 2.1 were visually estimated for the vegetation at each of the measurement locations.

The open section and vegetative barrier sections were at-grade ($\pm$ 2m) with the highway along the area of all six locations. An access road parallel to Interstate-280 was present along both the clearing and vegetation sections. This road provided access to measure air pollution concentrations

at the same distance from the highway for the clearing and behind barrier segments. The access road led to a small residential area, so fewer than 200 vehicles per day were estimated to use this road based on video surveillance collected during the study.

This study deployed two mobile monitoring vehicles equipped with air monitoring analyzers and portable sonic anemometers for meteorological measurements. One mobile monitoring vehicle was an electric car equipped with real-time location (with a global positioning system), black carbon (BC), particulate matter count (PM), nitrogen dioxide ($NO_2$), and carbon monoxide (CO) instruments that drove along the access road and measured air quality at each of the six fixed-site Stops as shown in Figure 2.1. For each day, the electric vehicle drove approximately 5 to 7 continuous laps along the access road and on Interstate-280. After the last lap, the sampling vehicle parked for 10-minutes at each of the six fixed-site Stops shown in Figure 2.1. All air quality instruments used in mobile monitoring measured at 1-second sampling intervals.

In addition to mobile monitoring, meteorological measurements were made approximately 20m from the nearest travel lane of Interstate-280. Meteorological measurements using three-dimensional (3-D) sonic anemometers provided information required to interpret the concentration measurements and evaluate the impacts of the vegetation barrier relative to the clearing location. One sonic anemometer was located at the clearing location approximately 2 m above ground, while three sonic anemometers were located on a tower behind the vegetative barrier at heights of 2, 3 and 5 meters above ground. The location of this tower was rotated among each of the behind-vegetation fixed sites each day. Thus, each location/vegetation barrier characteristic was monitored for four days.

A sport utility vehicle (SUV) was parked at Stop 1-CLEARING (approximately 20m from the highway) and continuously collected air quality measurements, including CO, NO, $NO_2$, and PM at 1-minute time intervals during this study. The measurements from the SUV in the clearing provided continuous comparisons between concentrations in the clearing and concentrations measured behind the vegetation with the electric vehicle. Batteries located within the vehicle powered these samplers, so the vehicle's engines could be turned off during all sampling times. Instrument calibrations were also performed each day before sampling began. At the end of each sampling day, the SUV and electric vehicle parked together to conduct co-located air monitoring

for a minimum of 30 minutes. Comparison of the collocated electric vehicle and SUV measurements showed highly correlated data collection, with $r^2$ values above 0.95.

## 2.3 Sacramento Study

A field study was conducted in Sacramento, California to examine the effect of tall vegetation behind a barrier on concentration levels in the vicinity of the highway. The study was conducted next to CA-99 in Sacramento (Figure 2.2). The freeway, which has an average traffic flow rate of 200,000 vehicles/day, is 42 m wide and has 10 lanes including 2 High Occupancy Vehicle (HOV) lanes. The barrier is 12 m from the edge of the highway, which is the only major source of pollution near the study area.

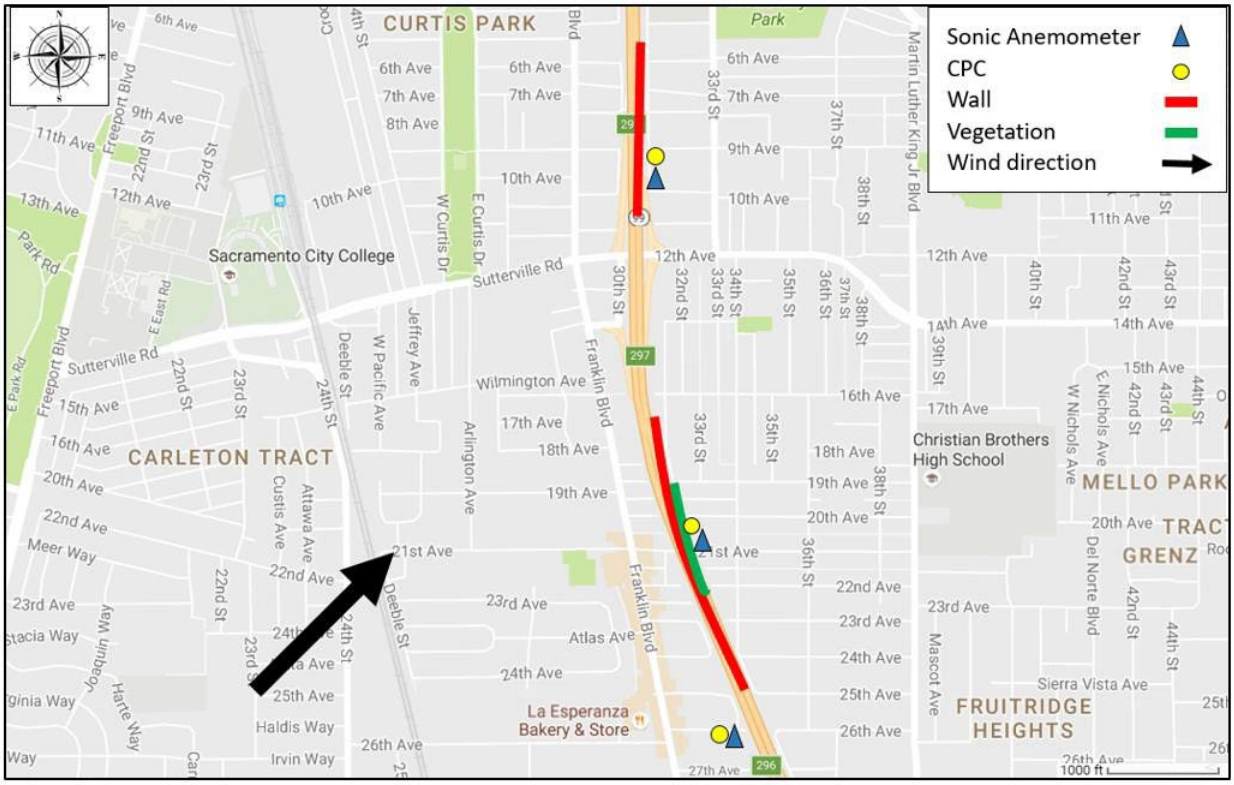


**Figure 2.2.** *Instrument locations*

The field study was conducted at two barrier sites (Figure 2.3). The first site has a 5 m barrier extending over 500 m on the east side of the highway. The other site has a barrier of the same height with tall trees planted behind it. The vegetation is a row of pine trees planted next to the

barrier extending over 200 m along the highway. The height of the trees is 15-18 meters. The freeway is at the same level behind the barriers at both sites.

At both locations, the areas downwind of the barriers are residential with one story houses. There are also streets behind the barriers at both locations, which made it possible to make measurements within 10 m from the barriers.

The primary pollutants for this measurement were Ultrafine particles (UFPs). UFPs have high concentrations near the highway and major urban sectors compared to background levels which make them good tracers for studying dispersion within these areas. There is also a strong association between UFP concentrations and adverse health effects (Pope III, 2002). Previous studies have shown that dispersion models can be developed to explain UFP concentration levels near major highways and urban areas (Amini et al., 2016; Schulte et al., 2015). Dispersion, deposition, and coagulation can decrease the concentration of UFPs, but the effects of coagulation and deposition are small within the short distances of the source (Zhang et al., 2004). So, the main mechanism for reducing concentrations is dispersion near the highway.

(a) (b)

**Figure 2.3.** *a) view of wall vegetation barrier. b) view of barrier and downwind anemometer behind it.*

UFP concentrations were measured with TSI Condensation Particle Counters (CPCs), Model 3022A. This model can measure concentrations in the range $5 \times 10^3$-$10^5$ particles/$cm^3$ with $\pm 10\%$ accuracy. Raspberry Pie Model 2B computers were configured to serve as data loggers for CPCs.

Meteorological variables were measured with Campbell Scientific CSAT3 3-D (three-dimensional) sonic anemometers, which have a resolution of 1 mm/s for horizontal velocity and 0.5 mm/s for vertical velocity. It also records temperature with a resolution of 0.025°C. Campbell Scientific CR1000, CR3000, and CR5000 dataloggers were used to record the data at 1 HZ. The sonic anemometers were powered with deep cycle marine batteries. The traffic flow in each lane

of the freeway was obtained from the CalTrans Performance Measurements System (www.pems.dot.ca.gov). Cars and trucks are treated separately in the data.

One CPC was located at each one of the downwind sampling locations, east of highway 99. The CPCs were installed inside two cars and powered by deep cycle marine batteries. Both cars were parked at 4 m behind the two locations, one downwind of the solid barrier, and the other downwind of the barrier with vegetation. The CPCs were interchanged each day to avoid instrumental error.

Another anemometer and CPC were located at the west side of the freeway at a house next to highway 99. One sonic anemometer was located at this location to measure temperature and wind velocities. An extra anemometer was used as a backup unit at the same location. Since the wind was blowing from the southwest most of the time, measurements at this location are considered as background. The anemometers were installed on a pole at 5 m above ground level (AGL).

The measurements were conducted on 21$^{st}$, 22$^{nd}$, 25$^{th}$, 26$^{th}$, 27$^{th}$, 28$^{th}$, and 30$^{th}$ of June 2016. The selected measurement period was 12:00–18:00 hours, during which time the wind blew primarily from the southwest. Since the highway is north-south, the wind that is perpendicular to the road is westerly. To avoid the effects of the interference between the two sections of the highway on downwind concentrations, we focused on data from June 25$^{th}$, 26$^{th}$, and 27$^{th}$, when the wind was westerly most of the time.

A sonic anemometer was installed at each of the downwind sampling locations to measure the effects of the solid and the solid-vegetation barriers on wind characteristics and turbulence levels. The sonic anemometers were installed on poles at 2.5 m above the ground and at 4 m downwind of the barrier sections.

Table 2.2 shows the time and date that each instrument was operational. Upwind sonic anemometers and CPC functioned throughout the measurement period. The data collection on July 27$^{th}$ and 28$^{th}$ were shortened due to malfunction of the downwind CPCs.

**Table 2.2.** *Overview of the dates and time of measurement.*

| Day # | Date | Downwind anemometers start time | Downwind anemometers stop time | Downwind CPCs start time | Downwind CPCs stop time |
|---|---|---|---|---|---|
| **1** | 6/21/2016 | --- | --- | 14:00 | 16:30 |
| **2** | 6/22/2016 | --- | --- | 13:00 | 15:00 |
| **3** | 6/25/2016 | 11:30 | 17:30 | 13:00 | 17:30 |
| **4** | 6/26/2016 | 11:30 | 16:00 | 11:45 | 16:00 |
| **5** | 6/27/2016 | 12:45 | 17:00 | 16:00 | 17:00 |
| **6** | 6/28/2016 | 10:45 | 14:30 | 12:30 | 14:30 |
| **7** | 6/30/2016 | --- | --- | 14:30 | 16:30 |

The results from the two field studies provided in data guidance in the development of VBM. The results from the Sacramento Study were used in the formulation of the models, while those from the Woodside Study were used in the evaluation of the proposed model.

## 2.4 References


- Ahangar, F. E., Venkatram, A., & Schulte, N. (2017). Reduction of air pollution levels downwind of a road with an upwind noise barrier. *Boundary-Layer Meteorology*, 165, 375–392. https://doi.org/10.1007/s10546-017-0280-7
- Al-Dabbous, A.N., Kumar, P., 2014. The influence of roadside vegetation barriers on airborne nanoparticles and pedestrian exposure under varying wind conditions. Atmos. Environ. 90, 113–124.
- Baldauf, R., Thoma, E., Khlystov, A., Isakov, V., Bowker, G., Long, T., Snow, R., 2008. Impacts of noise barriers on near-road air quality. Atmos. Environ. 42, 7502–7507.
- Baldauf, R. (2016). *Recommendations for Constructing Roadside Vegetation Barriers to Improve Near-Road Air Quality*. U.S. EPA, EPA/600/R-16/072. https://www.epa.gov/air-research/recommendations-constructing-roadside-vegetation-barriers-improve-near-road-air
- Baldauf, R. (2017). Roadside vegetation design characteristics that can improve local, near-road air quality. *Transportation Research Part D: Transport and Environment*, 52, 354–361. https://doi.org/10.1016/j.trd.2017.03.013
- Baldauf, R. W., Gantt, B., Deshmukh, P., et al. (2016). Influence of solid noise barriers on near-road and on-road air quality. *Atmospheric Environment*, 129, 265–276. https://doi.org/10.1016/j.atmosenv.2016.01.025
- Brantley, H. L., Hagler, G. S. W., Deshmukh, P., & Baldauf, R. (2014). Field assessment of the effects of roadside vegetation on near-road black carbon. *Science of the Total Environment*, 468–469, 120–129. https://doi.org/10.1016/j.scitotenv.2013.08.001
- Hagler, G.S.W., Lin, M.Y., Khlystov, A., Baldauf, R.W., Isakov, V., Faircloth, J., Jackson, L.E., 2012. Field investigation of roadside vegetative and structural barrier impact on near-road ultrafine particle concentrations under a variety of wind conditions. Sci. Total Environ. 419, 7–15.

- Setälä, H., Viippola, V., Rantalainen, A.-L., Pennanen, A., & Yli-Pelkonen, V. (2013). Does urban vegetation mitigate air pollution in northern conditions? *Environmental Pollution*, 183, 104–112. https://doi.org/10.1016/j.envpol.2012.10.015
- Tong, Z., Whitlow, T.H., MacRae, P.F., Landers, A.J., Harada, Y., 2015. Quantifying the effect of vegetation on near-road air quality using brief campaigns. Environ. Pollut. 201, 141–149. doi:10.1016/j.envpol.2015.02.026
- Vos, P., Maiheu, B., Vankerkom, J., & Janssen, S. (2013). Improving local air quality in cities: To tree or not to tree? *Environmental Pollution*, 183, 113–122. https://doi.org/10.1016/j.envpol.2012.10.021

# Chapter 3

## Formulation of Model

## 3.1 Results from Modeling Studies

Several modeling studies have been conducted to describe the effects of vegetative barriers on urban air pollution. Steffens et al. (2012) incorporated particle aerodynamics and deposition mechanisms into the Comprehensive Turbulent Aerosol Dynamics and Gas Chemistry (CTAG) model to examine the effects of vegetative barriers on roadway-emitted pollutants. They modeled the results of the field experiment conducted in Chapel Hill, NC (Hagler et al., 2012). They assumed that vegetative barriers affect near-road air quality in the following ways: 1) particles are deposited on leaf surfaces, 2) downwind wind speed and turbulence levels in the flow passing through the barrier are decreased, and 3) a fraction of the flow carrying pollutants is forced to go over the barrier. The first and third effects mitigate air pollution, while the second effect leads to higher concentrations. Another relevant Computational Fluid Dynamics (CFD) study conducted by Ghasemian, et al.(2017) shows that while dense vegetative barriers have a mitigating impact, low porosity barriers can increase concentrations by reducing wind speeds and hence turbulence in the flow passing through the barrier.

These CFD studies have provided valuable insight into the processes that govern the impact of vegetative barriers on dispersion of highway emissions. They have also been evaluated to a limited extend with data from field studies ( Deshmukh et al., 2019). However, their complexity and associated numerical demands make it inconvenient to apply them in a regulatory context where the model has to be relatively simple, transparent and has undergone extensive evaluation with field data. This has given rise to efforts (Isakov et al., 2016) to develop semi-empirical dispersion models that capture the essential features of the impact of vegetative barriers without demanding the computational resources of CFD models. In this project, we follow this approach in formulating VBM. VBM's design allows its incorporation into the framework of AERMOD, the USEPA recommended dispersion model, which currently accounts for the impact of both upwind and downwind solid barriers(Francisco et al., 2024) on near-road air quality.

## 3.2 Physical Processes Associated with Vegetative Barriers

Figure 3.1 depicts the processes that govern the transport and dispersion of highways emissions that encounter a vegetative barrier. Part of the flow goes through the porous vegetative barrier, and the rest goes over the barrier. The emissions carried with the flow going over the barrier are subject to enhanced vertical spread, similar to that in the presence of a sold barrier.

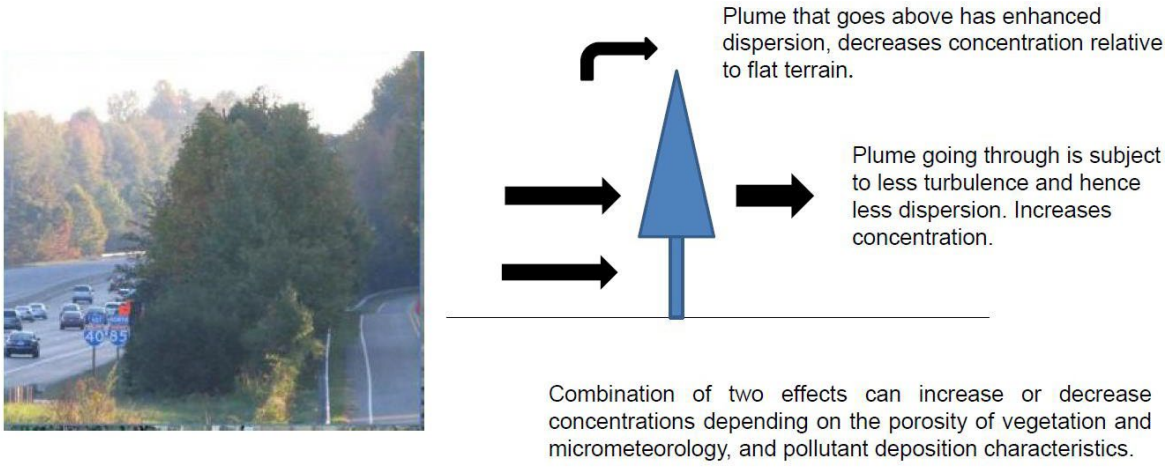


**Figure 3.1.** *Transport and dispersion of highway emissions in the presence of vegetative barriers.*

The effects of a vegetative barrier have been modelled using computational fluid dynamics where the barrier was treated as a continuous porous medium. These models show that such barriers reduce concentrations that would occur in the absence of a barrier. In principle, such models can be used to design barriers. However, these models are computationally cumbersome and require experts to apply them. The objective of this project is to develop and evaluate a model that is transparent to the user and can be readily applied by someone who is familiar with models such as AERMOD. We propose a dispersion model based on the idea that a vegetative barrier, to a first approximation, creates effects that lie between those of a solid barrier and those that occur in the absence of barrier. Then, the model can be written as:

$$C_v = (1-\varepsilon)C_b + \varepsilon C_f \alpha_t f_d \qquad (3.1)$$

where $C_v$ is the concentration downwind of the vegetative barrier, $C_b$ is the concentration at the same location downwind of a solid barrier with the same height as the vegetative barrier, and $C_f$

is the corresponding concentration in the absence of a barrier. So $C_v$ interpolates between the two possible limits of the concentration using the optical porosity, $\epsilon$, (Raupach et al., 2001) as the interpolating parameter. Optical porosity is readily measured using a photograph of the barrier and computing the fraction of the barrier that has "open" pixels. It is a measure of how much of the upwind emissions flow through the barrier; we realize that it might overestimate the "leakiness" of the barrier because it does not account for the role of the three-dimensional structure of the vegetation in obstructing flow.

The first term on the right-hand side of Equation (3.1) says that the flow that does not go through the barrier behaves as if it encounters a solid barrier, and the dispersion is governed by the model for solid barriers. The second term on the right says that the flow that goes through the barrier behaves like one in the absence of a barrier. The factor, $f_d$, accounts for dry deposition/impaction of pollutants in the barrier, and $\alpha_t$ accounts for the effects of the vegetation on turbulence.

The role of porosity on the impact of the vegetative barrier can be examined by neglecting the effects of dry deposition and turbulence modification to write:

$$C_v = (1-\varepsilon)C_b + \varepsilon C_f \tag{3.2}$$

where the barrier affected concentration is expressed using the simple formula equation (3.3) (Schulte et al., 2014):

$$C_b = \sqrt{\frac{2}{\pi}}\frac{q}{\sigma_w W}\ln\left(1+\frac{W}{\frac{H+x}{i_z}}\right) \tag{3.3}$$

where $q$ is the emission rate of the pollutant per unit length of the road, $W$ is the width of the road, $\sigma_w$ is the standard deviation of vertical velocity fluctuations near the surface of the road, $i_z$ is the corresponding turbulent intensity, and $x$ is the distance of the receptor from the edge of the road. The barrier affects the downwind concentration through the term, $H/i_z$, where $H$ is the height of the barrier: it effectively increases the downwind distance by $H/i_z$. So, its impact increases as the turbulent intensity, $i_z$, decreases, which suggests that the barrier is most effective when the near-surface boundary layer is stable, and least effective when the boundary layer is unstable. We can

model $C_f$, the concentration in the absence of the barrier by replacing the height of the barrier, $H$, by $h_0$, the vertical dispersion induced by vehicular motion.

Figure 3.2 compares the concentration reductions associated with the vegetative and solid barrier as a function of distance from the edge of the $40\ m$ wide road. The concentrations are normalized with those corresponding only to vehicle induced vertical dispersion, $h_0 = 2\ m$, and the downwind distance with the height of the barrier, $H = 5\ m$.

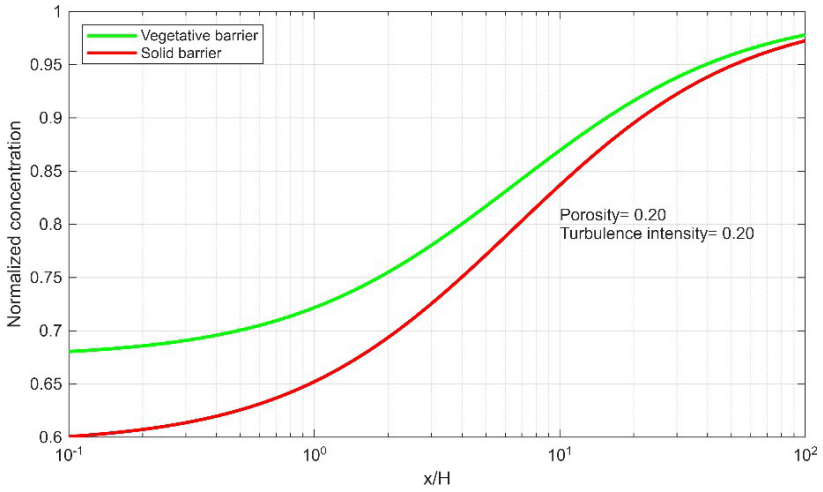


**Figure 3.2.** *Concentration reductions are associated with solid and vegetative barriers.* $\boldsymbol{H = 5\ m}$, $\boldsymbol{W = 40\ m}$

Figure 3.2 shows that the model, as it is formulated, results in the vegetative barrier having a smaller mitigating effect than the solid barrier. The reductions in concentrations associated with the vegetative barrier is about 70% close to the barrier and reduces to 5% at 50 times the barrier height, 200 m. It is important to note that these reductions only apply to the emissions from the road, and not to the total pre-barrier concentrations, which will include a background that might be several times the increment from the road. As we will see in the discussion of field studies, the presence of background concentrations can obscure these mitigating effects.

Figure 3.3 shows the effects of optical porosity and atmospheric turbulence intensity of the mitigating impact of vegetative barriers. The left panel shows that halving the porosity from 0.4 to 0.2 increases the reduction in concentrations, but this reduction is not proportionate going from 24% to 32%. Again, around 200 m from the edge of the road, both reductions approach about 2%. The right panel of Figure 3.3 shows that the mitigating effect of the barrier increases as the

turbulence intensity decreases. Near the road, the reduction increases from 20% to 24% as the turbulence intensity is reduced by a factor of two, 0.4 to 0.2. At the same time, the distance at which the reduction is 5% decreases from 30 to 10 m.

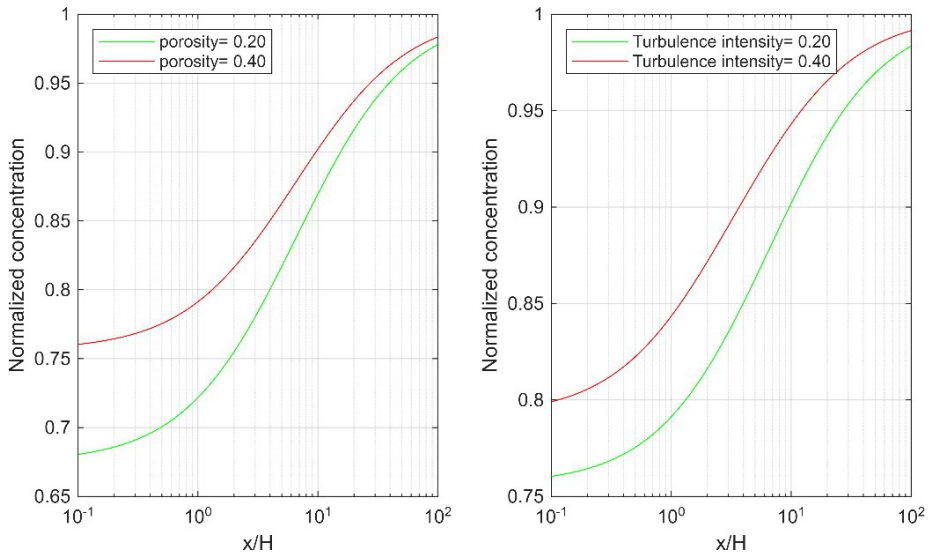


**Figure 3.3.** *The effects of porosity and atmospheric turbulence intensity of the impact of vegetative barriers on concentrations* $\boldsymbol{H = 5\ m}$, $\boldsymbol{W = 40\ m}$.

We can examine the effects of dry deposition on the vegetation barrier by depicting the barrier as a porous medium in which clear tubes are laid along the width of the barrier, denoted by $R$ in Figure 3.4.

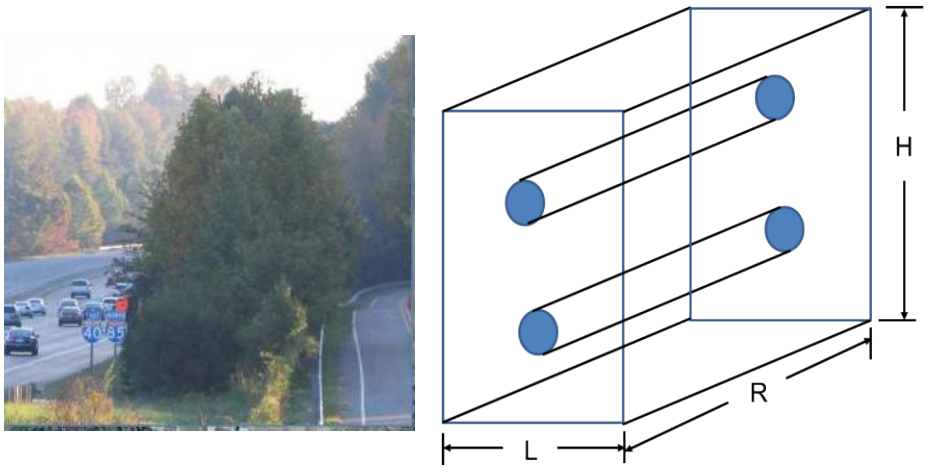


**Figure 3.4.** *Schematics used to derive the dry deposition factor,* $\boldsymbol{f_d}$.

Consider a section of the barrier that has length, $L$, and height, $H$, facing the wind. The tubes of radius, $r$, are laid along the width $R$ of the barrier. Assume that there are $n$ tubes in the area $L.\ H$. In this model, the porosity $\epsilon$ is related to the frontal area occupied by the hollow tubes through

$$n\pi r^2 = \varepsilon LH \tag{3.4}$$

and the inner surface area of the tubes is related to the Leaf Area Index (LAI) through the equation

$$n2\pi rR = 2(LAI)RL \tag{3.5}$$

where $LAI$ is Leaf Area Index defined as the one-sided leaf area in a block of vegetation divided by the projected area of the block on the ground. The factor on the right-hand side of Equation (3.5) accounts for two sides of a leaf. Dividing Equation (3.4) by (3.5) yields the expression for the radius, $r$, of the tubes

$$r = \frac{\varepsilon H}{LAI} \tag{3.6}$$

Now we are in a position to write the mass balance of a pollutant that is carried with the flow through the vegetation. If the flow velocity is $u$ and the deposition velocity of the pollutant is $v_d$, the mass balance in terms of the concentration can be written as

$$\frac{dC}{dy} = -\frac{v_d}{u}\frac{2}{r}C \tag{3.7}$$

where $y$ is the distance along the modeled tube. Integrating this equation, and substituting for $r$ from Equation (3.6), we obtain the expression for $f_d$,

$$f_d = \frac{C(y=W)}{C(y=0)} = \exp\left(-2\left(\frac{v_d}{u}\right)\left(\frac{LAI}{\varepsilon}\right)\left(\frac{W}{H}\right)\right) \tag{3.8}$$

This expression is likely to underestimate $f_d$ because $\epsilon$ might overestimate the leakiness of the vegetation, $W$ might underestimate the "tortuous" path taken by the air through the barrier, and the flow though the barrier, $u$,is likely to be smaller than the incoming ambient velocity. Realizing these uncertainties, it is still useful to examine its value as a function of the variables in Equation (3.8). Figure 3.5 shows this variation of $f_d$ . Note that dry deposition velocities of gases and small particles rarely exceed 2 cm/s. We see that dry deposition is a mitigating factor at low porosities;

however, the main reduction mechanism is enhanced vertical dispersion because only a small fraction of the flow goes through the vegetation when the porosity is low.

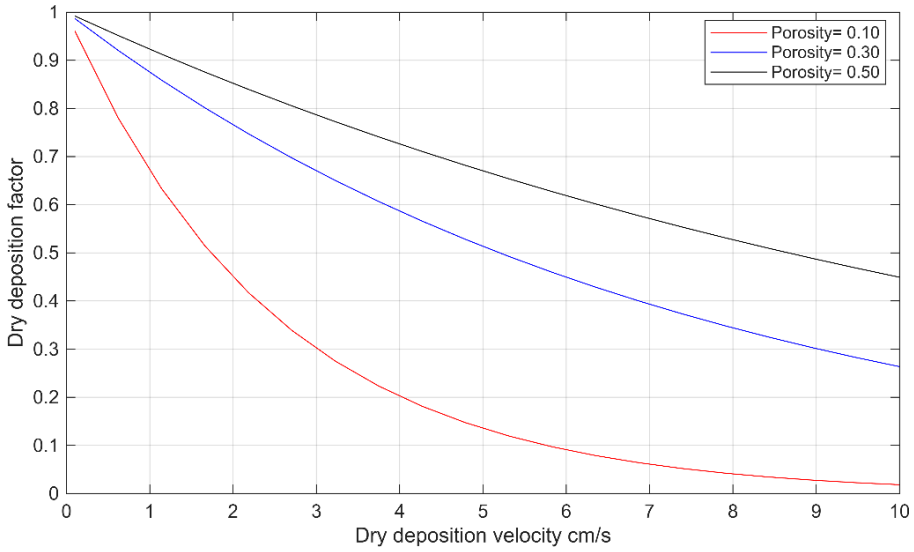


**Figure 3.5.** *Variation of* $\boldsymbol{f_d}$ *with deposition velocity and porosity.* $\boldsymbol{H = 5\ m, LAI = 5, u = 1\ m/s}$

The impact of deposition on barrier-induced mitigation is illustrated in Figure 3.6. As in the previous cases, the mitigation effect decreases with distance from the road, but the initial reduction associated with deposition persists with distance; the difference in this case is the additional 5% reduction caused by deposition. Note that the majority of the mitigating effect is related to the enhancement of vertical dispersion by the vegetative barrier. In Chapter 5 , we evaluate the proposed model with data from a field study that we conducted.

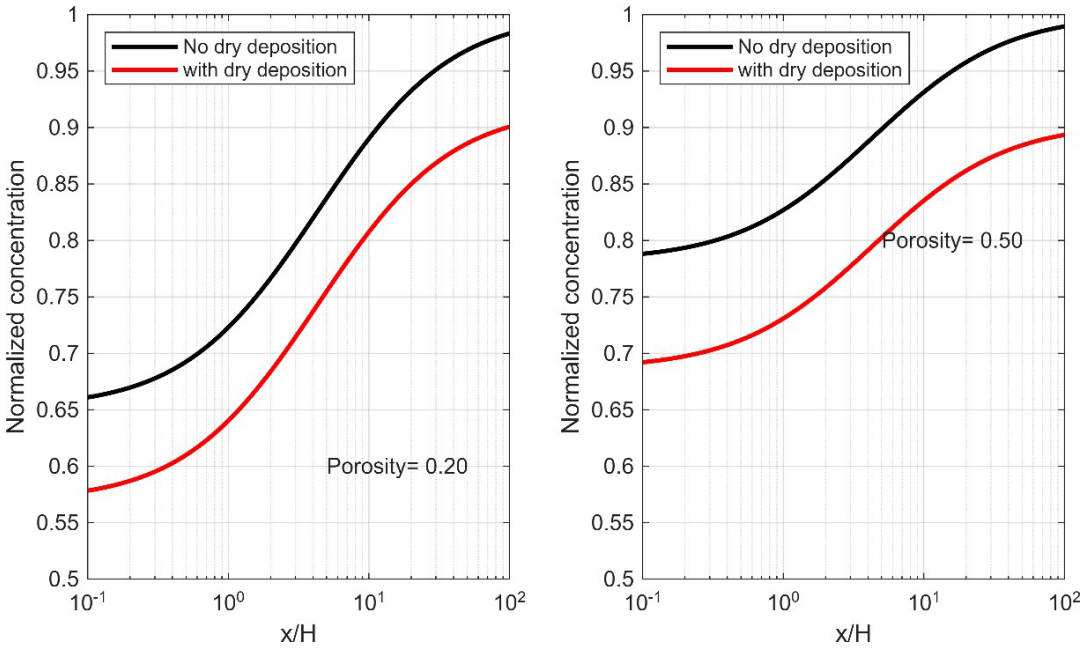


**Figure 3.6.** *Impact of deposition on normalized concentrations.* $\boldsymbol{H = 5\ m, v_d = 2\ cm/s}$, $\boldsymbol{W = 2\ m, LAI = 5, u = 1\ m/s}$.

We provide a brief description of the solid barrier treatment in AERMOD, which is a component of the dispersion model for the vegetative barrier. Note that the model also applies to flat terrain when the barrier height is set to zero.

## 3.3 SOLID BARRIER MODEL

Figure 3.7 depicts the processes incorporated into the solid barrier model: lifting of the plume above the barrier followed by the entrainment of material in the plume into the wake downwind of the barrier. The plume from the source is first dispersed from its source neglecting the presence of the barrier. At the barrier, the vertical concentration profile resulting from dispersion upwind of the barrier is lifted to the top of the barrier by simply changing the vertical coordinate system used in describing the release so that the origin is at the top of the barrier: the new coordinate $z' = z - h_o$, where $h_o$ is the barrier height.

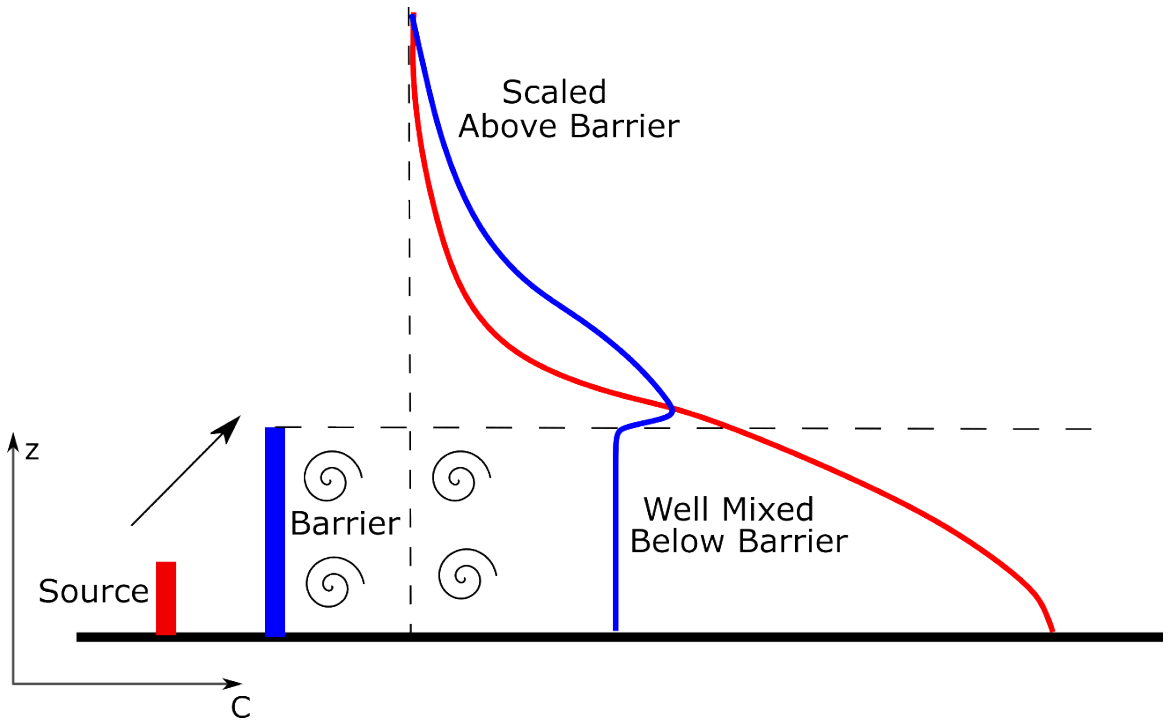


**Figure 3.7.** *Schematic showing the vertical concentration distribution of the scaled barrier model. The swirls indicate the recirculation zone formed behind the barrier and the inclined arrow indicates the lifting of the plume up to the barrier height. The well-mixed layer below the barrier and scaled concentration above it are shown by the blue line while the red line represents the distribution without any barrier.*

The entrainment into the wake is modeled by scaling the concentration profile above the barrier by a factor $f_q < 1$ to account for the mass flux below the barrier. The vertical distribution beyond the barrier is given by

$$F_z(x_d, z\phi) = \frac{f_q}{\sqrt{2\pi}\, U_e \sigma_z} \left[ \exp\left(-\frac{(z_s - z\phi)^2}{2\sigma_z^2}\right) + \exp\left(-\frac{(z_s + z\phi)^2}{2\sigma_z^2}\right) \right]; \quad z > h_o \tag{3.9}$$

$$F_z(x_d, z\phi) = f_e f_q F_z(x_d, 0); \quad z \le h_o$$

where $x_d$ is the effective distance downwind of the barrier, $\sigma_z$ is the vertical plume spread at this distance, $U_e$ is the effective horizontal velocity above barrier height and $f_e$ is the entrainment factor. The calculation of these parameters is described later.

Note that the concentration below barrier height is constant. If the entrainment factor $f_e = 1$, the concentration is continuous across $z = h_o$. A value $f_e < 1$ results in a discontinuity in the concentration at the top of the barrier; this mimics the sharp increase in concentration at the top of

the barrier measured in wind tunnel simulations (Heist et al., 2009). The scaling factor, $f_q$, can be derived from a mass balance based on unit emission rate from the source,

$$f_q + f_q f_e F_z(x_d, 0) U_b h_o = 1 \tag{3.10}$$

where the first term on the left-hand side is the horizontal mass flux above the barrier, and the second term is the flux below the barrier. The uniform velocity below barrier height, $U_b$, is taken to be the average velocity below the barrier height. The velocity profile is based on Monin-Obukhov similarity theory, where the values of the roughness length, $z_o$, the friction velocity, $u_*$, and the Monin-Obukhov length, *L*, are based on upwind micrometeorological measurements modified to account for barrier effects as discussed later.

Equation (3.10) yields

$$f_q(x_d) = \frac{1}{1 + f_e F_z(x_d, 0) U_b h_o} \tag{3.11}$$

The formulation for $f_e$ is discussed in the next section.

The concentration profile with and without the barrier are shown in Figure 3.7. The concentration below the barrier height is constant and is lower than the concentration without the barrier. Above the barrier height, the concentration distribution follows a Gaussian profile: $f_q F_z(x_d, z)$. Note that the concentration profile assumes its near ground release shape when the barrier height, $h_o = 0$. Also, the effect of the barrier becomes small as $F_z(x_d, 0)$ becomes small at large downwind distances.

In the model, the highway is represented as a set of line sources corresponding to the lanes on the highway. The contribution from each line source to the concentration at a receptor when the wind is not perpendicular to the line source is obtained from the approximate expression (Venkatram and Horst, 2006),

$$C(x, y, z) = \frac{q}{\cos(q)} \left( erf(t_1) - erf(t_2) \right) F_z(x_d, z\phi) \tag{3.12}$$

$$t_i = \frac{y_i - y}{\sqrt{2}s_y(x - x_i)} \tag{3.13}$$

where $q$ is the line source emission rate per unit length of the road, $x$ and $y$ are the receptor coordinates based on the coordinate system in which the x-axis is parallel to the wind direction, 1 and 2 correspond to the endpoints of the line source, $q$ corresponds to the wind direction with respect to the x-axis, $y - y_i$ is the distance of the endpoints from the receptor along the direction perpendicular to the wind direction, $s_y(x - x_i)$ is the horizontal plume spread (Venkatram et al., 2013b) at the distance of the receptor from the two endpoints along the direction parallel to the wind, and $F_z(x_d, z\phi)$ is the vertical distribution function discussed earlier. The effective downwind distance from the barrier $x_d$, is the shortest distance along the wind direction between the receptor and the barrier.

The effective wind velocity, $U_e$ in Equation (3.9) is given by

$$U_e = \sqrt{\left(2s_v^2 + U(\bar{z} + h_o)^2\right)} \tag{3.14}$$

where $U(\bar{z})$ is the average vector wind speed at the mean plume height, $\bar{z}$. The mean plume height, $\bar{z}$, is related to the vertical plume spread, which in turn is a function of $U_e$. So these parameters are computed iteratively (Venkatram et al., 2013b) from

$$s_z = f\left(x, u_*, L, U_e(h_o)\right) \tag{3.15}$$

where:

$$f(x, u_*, L, U_e) = \begin{cases} 0.57\dfrac{u_*}{U_e}\left(1 - 1.5\dfrac{u_*}{U_e}\dfrac{x}{L}\right)^{\frac{1}{3}}; L < 0 \\ 0.57\dfrac{u_*}{U_e}\left(1 + 3\dfrac{u_*}{U_e}\dfrac{x}{L}\right)^{-1}; L > 0 \end{cases} \tag{3.16}$$

$$\bar{z} = s_z\sqrt{\frac{2}{p}}\exp\left(-\frac{1}{2}\left(\frac{z_s}{s_z}\right)^2\right) + z_s\, erf\left(\frac{z_s}{\sqrt{2}s_z}\right) \tag{3.17}$$

Equation (3.12) breaks down when $q = 90^{o}$ because of the $\cos q$ in the denominator. The term $s_z \cos q$ (Venkatram et al., 2013a) is modified as follows to avoid this,

$$s_z(x_d)\cos q = \frac{s_z(x_d \cos q) + s_z(x_d)\cos q}{2} \tag{3.18}$$

Vertical mixing occurs when the plume travels from the line source to the barrier. This mixing is also enhanced by the movement of vehicles on the freeway. The vertical plume spread due to this vertical mixing is added to the vertical spread between the line source and barrier,

$$s_{z0} = \sqrt{s_z(x_s, u_*, L, U_e(0))^2 + h_v^2} \tag{3.19}$$

where $x_s$ is the downwind distance from the line source to the barrier and $h_v$is the effective height of the vehicles traveling on the freeway. Then, the vertical spread between the source and barrier is accounted for in the vertical spread downwind of the barrier through a virtual distance, $x_0$, computed from the implicit equation

$$s_{z0} = f\left(x_0, u_{*b}, L, U_e(h_o)\right) \tag{3.20}$$

where $u_{*b}$ is the friction factor that accounts for enhanced turbulence downwind of the barrier. The virtual distance, $x_0$, is added to the downwind distance, $x_d$. from the barrier to the receptor.

### 3.3.1 $u_*$ Correction

The presence of the barrier increases turbulent mixing downwind of the barrier as measured in various studies (Heist et al., 2009). This increase in turbulence is accounted for by increasing the friction velocity, $u_*$ near the barrier as follows,

$$z_{ob} = \max\left(\frac{h_o}{\sqrt{9}}, z_o\right) \tag{3.21}$$

$$u_{*b} = u_* \left(\frac{z_{ob}}{z_o}\right)^{0.17} \tag{3.22}$$

The friction velocity was used to compute a modified Monin-Obukhov length assuming that the heat flux does not change. The modified friction velocity, $u_{*b}$ recovers to its upwind value over a length scale determined empirically to be $5h_o$. Then,

$$u_{*c} = u_{*b} f_m + u_* \left(1 - f_m\right) \tag{3.23}$$

$$f_m = \exp\left(-\frac{x_d}{5h_o}\right) \tag{3.24}$$

where $u_{*c}$ is the corrected friction velocity used in computing vertical spread of the plume. The factor $f_m$ tends to 1 near the barrier and zero at downwind distances that are several times the height of the barrier.

## 3.3.2 Entrainment Factor, $f_e$

When the wind speeds are low, the model overestimated concentrations in a field study(Thiruvenkatachari et al., 2022), which suggested decreasing the entrainment factor, $f_e$, to values below unity in this situation. This suggested the following empirical relation,

$$f_e = \frac{u_{*b}}{u_{*b} + u_{*o}} \tag{3.25}$$

where $u_{*o} = 0.1$ m/s. $f_e$ tends to 1 as $u_{*b}$ increases. Equation (3.25) is designed to reflect the possibility that the turbulence generated by wind shear at the top of the barrier becomes less effective in entraining the plume above the barrier as the wind speeds approach zero.

# Chapter 4

## Field Studies

## 4.1 Introduction

Data from past field studies. Described Chapter 2, provided information that helped in the development of VBM. However, the information was not complete enough to evaluate the performance of the model. This motivated us to conduct several field studies in 2023 and 2024. These studies were not successful in that they did not allow us to reach definite conclusions on the impact of vegetative barriers. The major impediment to success was this: because the contribution of highway emissions of the major tracers, PM2.5 and PM10, to the measured concentrations was small compared to the background levels, it was difficult to isolate the impact of the vegetative barrier using the instrumentation that was available to us. It was only in late 2024 and in 2025 that we produced a strategy to isolate barrier effects in the midst of variations in background levels. So, most of this chapter will be devoted to field studies based on this strategy. We will provide brief descriptions of the studies that did not lead to successful results.

## 4.2 Instrumentation

The experimental setup employed three primary instruments to characterize particulate matter, black carbon concentration, and micrometeorological conditions. These included a PurpleAir Flex optical particle monitor, a Campbell Scientific CSAT3B three-dimensional sonic anemometer, and a microAeth AL30 aethalometer. Each instrument contributed measurements essential for interpreting atmospheric processes and emission or dispersion behavior during the study period.

### 4.2.1 PurpleAir Flex Particulate Matter Sensor

The PurpleAir Flex is a compact, dual-laser optical particle counter used to monitor ambient particulate matter in real time. The instrument incorporates two Plantower PMS-6003 sensors, which count particles in multiple size bins (0.3–10 μm) and derive mass concentrations such as $PM_{2.5}$. The device also integrates a Bosch BME688 environmental sensor for measuring temperature, pressure, relative humidity, and total volatile organic compounds. The PurpleAir

supports both Wi-Fi connectivity for continuous cloud-based data streaming and onboard SD-card logging for offline acquisition. Its small size and low-power design make it suitable for outdoor deployments requiring high spatial or temporal resolution. In this experiment, the PurpleAir Flex provided continuous time-series measurements of particulate matter to evaluate ambient variability and near-source PM behavior.

### 4.2.2 CSAT3B Three-Dimensional Sonic Anemometer

The Campbell Scientific CSAT3B is a research-grade sonic anemometer designed to measure three-dimensional wind components (u, v, w) and sonic temperature at sampling rates up to 100 Hz. The instrument determines wind velocity by transmitting and receiving acoustic pulses across three orthogonal paths, with the speed of sound providing temperature estimates. The CSAT3B features an integrated electronic design, a 10-cm measurement path, and minimal flow distortion, making it suitable for turbulence and eddy-covariance applications. In this experiment, the CSAT3B was used to characterize local micrometeorological conditions, including wind speed, wind direction, and turbulent fluctuations. These measurements were essential for interpreting pollutant transport, atmospheric mixing, and short-term dispersion patterns.

### 4.2.3 microAeth AL30 Black Carbon Monitor

The AethLabs microAeth AL30 is a portable, battery-powered aethalometer used to quantify black carbon (BC) concentration using optical absorption at 880 nm. Ambient air is actively drawn through a PTFE filter, and changes in light attenuation are converted to real-time BC concentrations at user-selectable time intervals. The AL30 includes an integrated pump, flow controller, data logger, and onboard storage, enabling fully autonomous operation in both stationery and mobile deployments. Its small size and low flow rates (typically 50–250 mL/min) make it well suited for exposure studies, near-source monitoring, and urban air-quality characterization. In this experiment, the AL30 provided high-resolution black carbon measurements to evaluate combustion-related aerosol contributions and identify temporal variations linked to traffic or other local sources.

## 4.3 Studies at UCR Agricultural Station

We conducted a series of experiments at the UCR Agricultural Station, Riverside, to examine the impact of orange trees on reducing particulate concentrations originating from the adjoining road. The trees are planted in rows perpendicular to Chicago Street and Iowa streets, which run North-South, as shown in the top panel of Figure 4.1. The wind direction during the day is westerly. PurpleAir particulate matter sensors were mounted behind the trees and between the rows, as shown in Figure 4.1. The locations of the sensors and the sonic anemometer are shown in Figure 4.2.

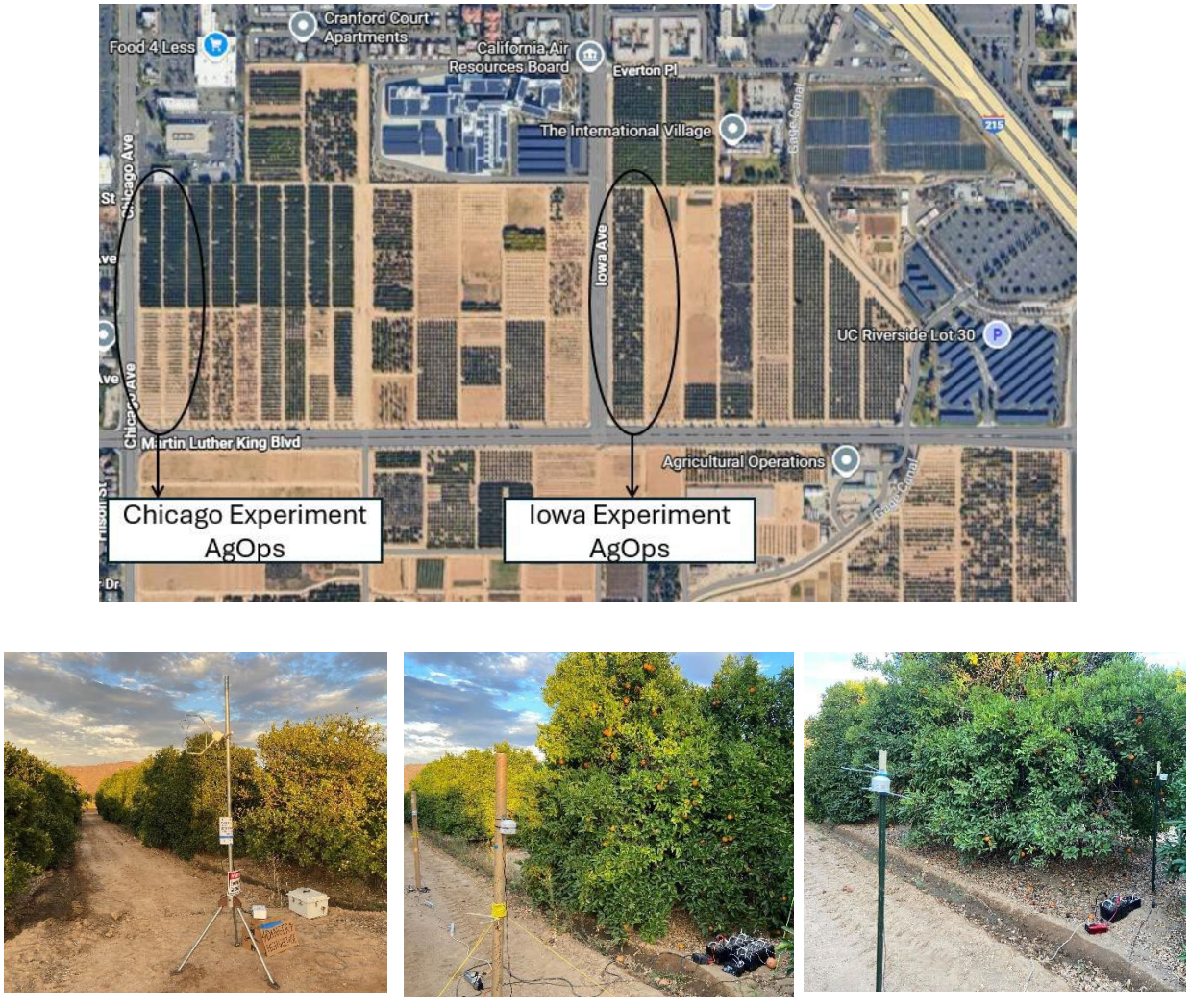


**Figure 4.1.** *Typical setup of studies conducted at the UCR Agricultural Station. Top panel shows the location on Iowa Avenue, Riverside, CA. Bottom panel shows mounting of the PurpleAir sensors between tree rows.*

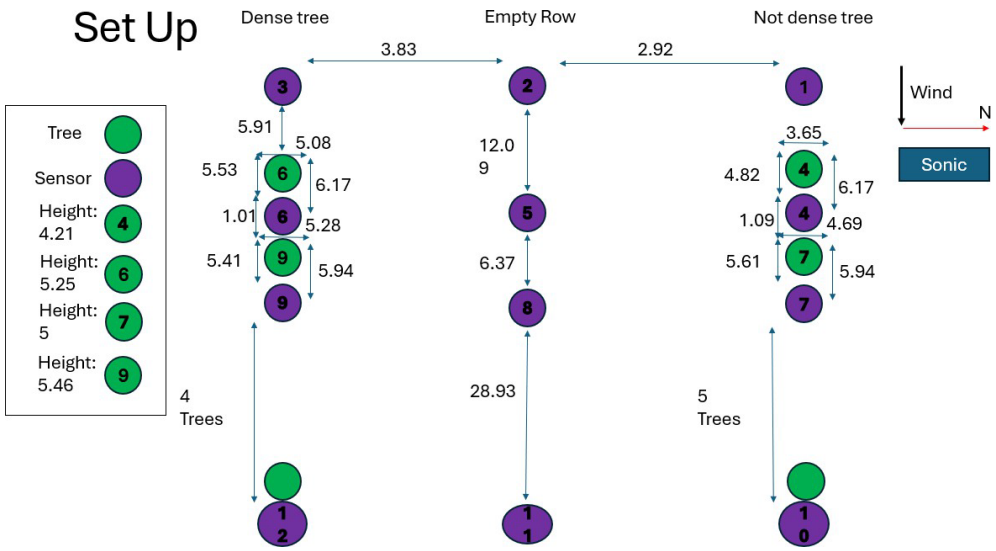


**Figure 4.2.** *Locations of sensors at the UCR Agricultural Station on Chicago Avenue.*

The objective of the experiments was to measure the differences in concentration patterns along the three rows shown in Figure 4.2, and then use the measurements to develop a dispersion model. We first conducted experiments on Iowa Avenue and then moved to Chicago Avenue to examine the possibility that higher traffic flows on Chicago would result in higher PM emissions and hence more separation of vegetative barrier effects from background variations.

The measurements at Iowa and Chicago did not show any systematic differences between the concentration patterns measured along the trees and the empty row. Suspecting that the wind flow pattern was affected by the empty rows between the tree rows, we closed the space between the trees using plastic sheets as shown in Figure 4.3. This modification did not improve our ability to isolate the impact of vegetative barriers. Such results motivated our shift to a different approach to conducting field studies, which is described next.

**Figure 4.3.** *Gaps between trees covered with plastic sheets.*

## 4.4 Field Studies on Highways

### 4.4.1 Identifying a field location

The focal field site was selected after an extensive review of roadside vegetation using the street view of either Google maps, Bing map, or Apple maps. Highways that run north to south were the focus of this review (Highways: 2, 5, 23, 55, 57, 71, 110, 163, 210, 215, 261, 405, 605, 710). Despite the extensive network of freeways in southern California few areas have continuous stretches of vegetation that would be represented of an "effective" vegetation barrier as identified by Baldauf 2017. Roadside vegetation was commonly observed as spaced single plants, low lying shrubs, vegetation along a slope, covering an existing concrete wall, or extending above a concrete wall. Few locations offered the conditions needed to be an experimental site.

Only one location on SR-55 offered features that allowed collection of data suitable for the evaluation of VBM. The site, shown in Figure 4.4, located just south of SR-91, has features that make it uniquely suitable for this study:

1. SR-55 runs almost north-south, which allows the impact of the east-located barriers to be studied during the dominant day-time westerly winds at this location.
2. The site has two types of barriers, and an open area, shown in the bottom panel of Figure 4.4. This allows direct comparison of the impact of highway emissions on concentrations

downwind of the solid and the vegetative barrier. The open area allows us to account for the effects of atmospheric dispersion by making this comparison.

3. The area downwind of the barriers is a parking lot shared by several small businesses. This allowed us to park the mobile platform at distances of a few meters downwind of the barriers.

4. The area upwind of the highway was relatively open, which allowed the placement of sonic anemometers to measure meteorology and instruments to measure background concentrations.

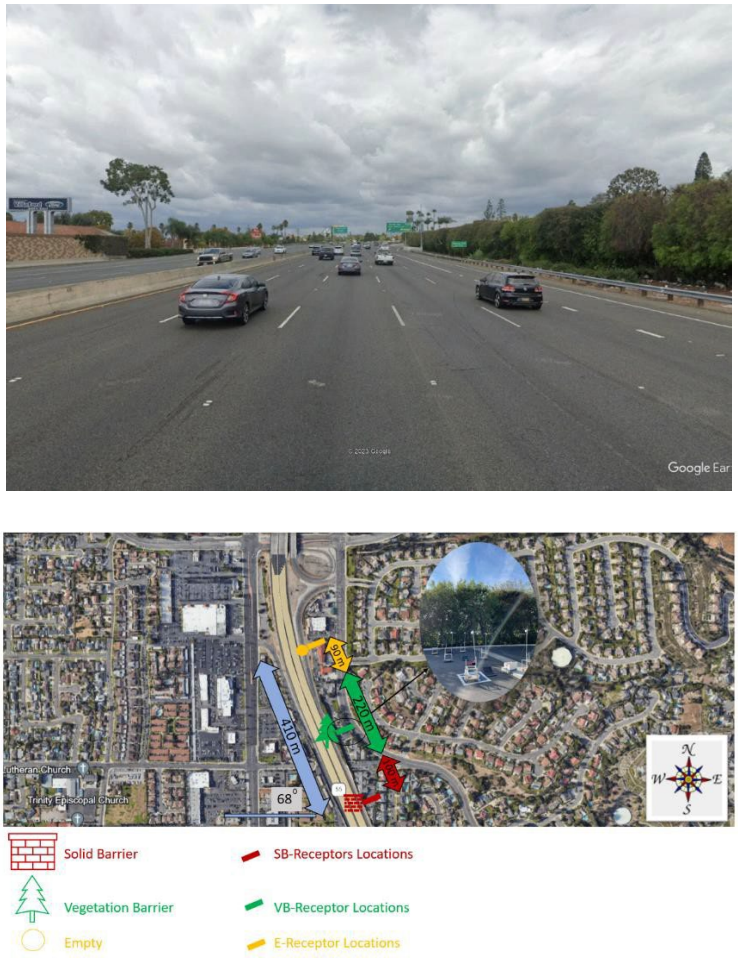


**Figure 4.4.** *Two views of the SR-55 site at which field studies were conducted in 2024 and 2025. Top view shows the highway from the point of view of an observer looking north. The vegetative barrier is on the right. The bottom panel is an aerial view that shows the three sections: solid barrier, vegetative barrier, and open area.*

### 4.4.2 Overview of field studies

Our first set of experiments used several PurpleAir monitors to measure PM concentrations at several locations downwind of the three kinds of barriers-solid, vegetative, and open-to detect differences in concentration patterns (Figure 4.5). The results from these studies were difficult to interpret because the mitigating effect of the barrier was minor compared to the background concentrations of particulate matter. The precision of the instruments used to measure concentrations upwind and downwind of the barriers did not allow us to capture these differences.

**Figure 4.5.** *Set up of initial experiments at SR-55. PurpleAir sensors placed at several downwind locations.*

In the most recent field studies, conducted in 2024 and 2025, we decided to avoid this problem with instrument precision by using one instrument or two instruments mounted on a mobile platform to make measurements at different locations along SR-55 and then comparing them to estimate the effects of barriers on near-road concentrations of particulate matter. This meant that we could not make simultaneous measurements at these locations to estimate differences between concentrations upwind and downwind of barriers. Thus, we assumed that average concentration did not vary significantly during the time that the mobile sampling was conducted. This assumption introduces uncertainty in the analysis of the data.

The studies were conducted by driving the mobile platform first along the highway on the rightmost lane heading north, exiting the highway to stop at three locations for ten minutes at each location, and then getting back on the highway to complete the loop. About two loops were completed each hour. Sampling during a typical day lasted about two to five hours during the

daytime. Meteorological information was continuously measured using sonic anemometers located upwind and downwind of the highway at locations shown in Figure 4.6.

**Figure 4.6.** *Left panel shows downwind sonic anemometer located in the open section. Right panel shows upwind sonic located west of SR-55.*

### 4.4.3 Estimating vegetative barrier attributes


**Figure 4.7.** *Aerial view of three sampling locations from Fall 2025 along the SR-55 vegetation barrier.*

At the SR-55 study site four different vegetative attributes that influence dispersion were measured – Height, Width, Leaf Area Index and Porosity. Height was measured via the trigonometric principle used by forestry inventory methods (Figure 4.8). Width was measured perpendicular to the length of the barrier. Leaf Area Index (LAI), the area of leaves per unit area, was measured using the AccuPAR LP-80 (Decagon Devices, Inc.). The AccuPAR calculates LAI using the above and below-canopy photosynthetically active radiation, along with variables that relate to the canopy architecture and position of the sun. LAI was measured approximately 1.25 m from the soil surface, as this best represented the height at which the mobile sensors were sampling. LAI values close to 0 indicate low vegetation canopy and higher values indicate denser vegetation canopies.

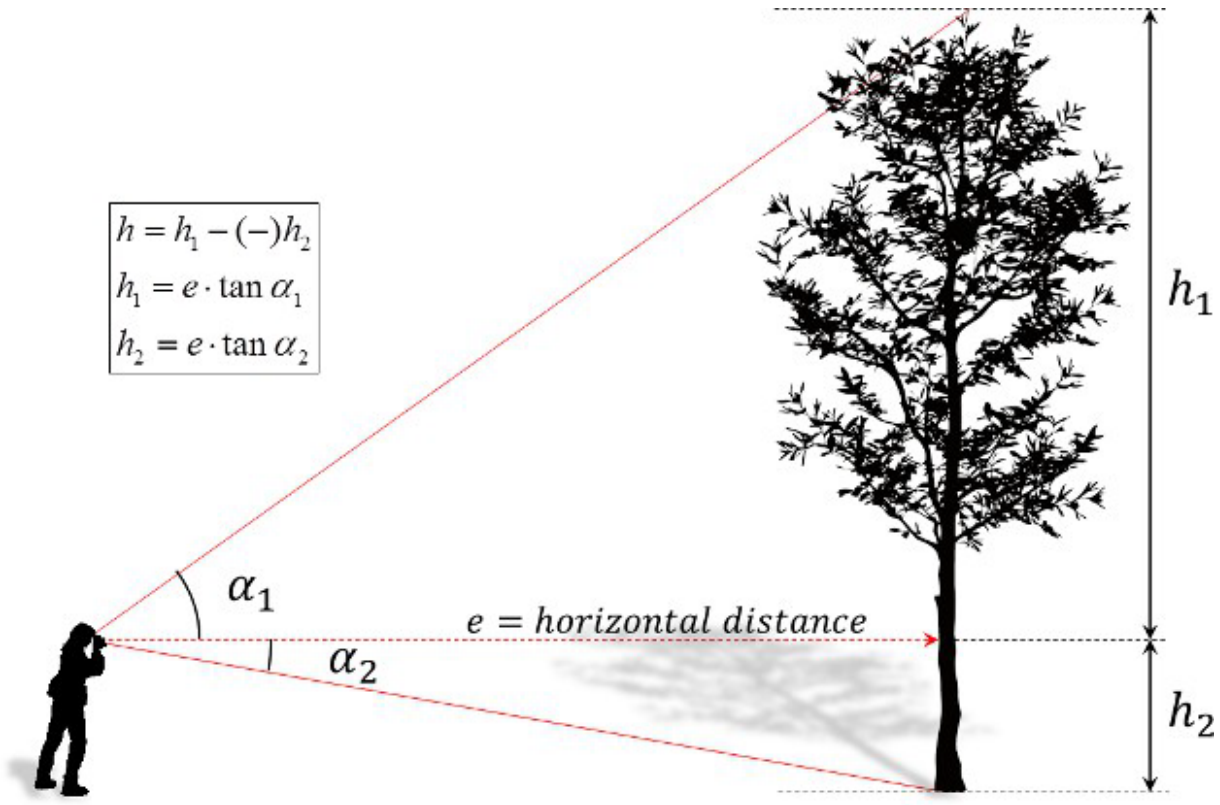


**Figure 4.8.** *Schematic of the trigonometric principle used to estimate vegetative barrier height.*

Porosity was estimated from RGB photographs using the software ImageJ. Briefly, the red, green, blue color thresholds were adjusted so that the entire image was set to a red threshold, the hue, saturation, and brightness were adjusted so that the vegetative plant material remained red (Dunn

and Martin 2004). Optical Porosity was estimated based on the proportion of the vegetation pixels within the total pixels of an image; specifically, we define the optical porosity $\varphi_{opt}$ of an image region $\Omega$ as:

$$\phi_{opt} = \frac{A_{void}}{A_{\Omega}} = 1 - \frac{A_{veg}}{A_{\Omega}} \tag{4.1}$$

where $A_{veg}$ and $A_{void}$ are vegetation and void pixel areas, respectively. We multiply this number by 100 to get a percentage (Table 4.1). Estimating $A_{veg}$ can be difficult over an entire image, therefore the 9 m section of the sampled vegetation barrier was divided into three 3 m sections. Optical porosity can also vary vertically due to differences in plant species or landscape maintenance; therefore, we further divided the vegetation barrier into an upper and lower half with the lower half being up to 4 m and upper 4 m and above (Figure 4.9).

**Figure 4.9.** *Example of how a 9 m section of the vegetative barrier was divided to estimate porosity and species composition.*

**Table 4.1.** Summary of the estimates and process of estimating optical porosity for the three sampling locations at SR-55.

| Location | Sample Date | Porosity Estimate | Full 9 m section | Original 3-6 m | Processed 3-6 m ($A_{veg}$) |
|---|---|---|---|---|---|
| **Stop 1** | November 2025 | 50.78% |  |  |  |
| **Stop 2** | November 2025 | 38.15% |  |  |  |
| **Stop 3** | September 2025 | 41.42% |  |  |  |

The vegetation barrier was composed of four different species of shrubs: Elm - *Ulmus parviflora*, Pepper Tree - *Schinus molle*, Holm oak - *Quercus ilex* and Shiny xylosma -*Xylosma congestum* (Figure 4.10). At each of the three stops, the composition of the vegetation was estimated visually for three sections the lower half, upper half and the entire 9 m section as the most abundant species varied between the lower and upper half.

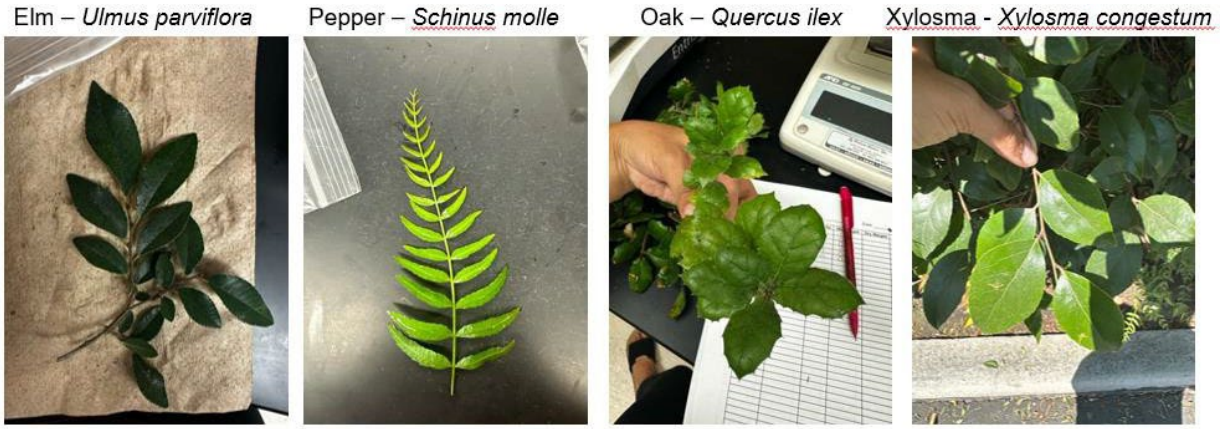


**Figure 4.10.** *Pictures of the leaves of the four species present along the SR-55 vegetation barrier.*

### 4.4.4 Summary of Vegetative Attributes.

The three sampling locations ranged in height from 6.21 to 9.1 m with the average height of the 3 sampling locations being between 7 and 8 m (Table 4.2). The width of the barrier was only measured at Stop 1 due to the presence of unhoused individuals at the other two stops. The LAI values were overall low for the three sampling locations but tended to increase with decreasing porosity and increasing barrier height. Porosity values were likely also impacted by the plant species of the barrier (Figure 4.11). For example, the upper half of the barrier for Stop 1 and Stop 3 was dominated by Pepper Tree (*Schinus molle*), which tends to have a more open canopy than Holm Oak (*Quercus Ilex*), which made up the upper half of Stop 2. Notably, the lower half of the barrier was overwhelming composed of Shiny Xylosma (*Xylosma congestum*), but the overall condition of the plant differed along the barrier with Stop 1 having more gaps. Both observations suggest that maintenance and the condition of a plant as well as the plant's identity will influence the attributes that will influence the efficacy of a vegetative barrier.

**Table 4.2.** *Average vegetative attributes of the three sampling locations from Fall 2025 along the SR-55 vegetation barrier. LAI – Leaf Area Index*

| Location | Sampling Date | Height (m) | Width (m) | LAI | Porosity |
|---|---|---|---|---|---|
| **Stop 1** | November 2025 | 7.2 | 4.62 | 0.82 | 50.78% |
| **Stop 2** | November 2025 | 7.7 | 4 | 1.91 | 38.15% |
| **Stop 3** | September 2025 | 8.3 | 4 | 2.66 | 41.42% |

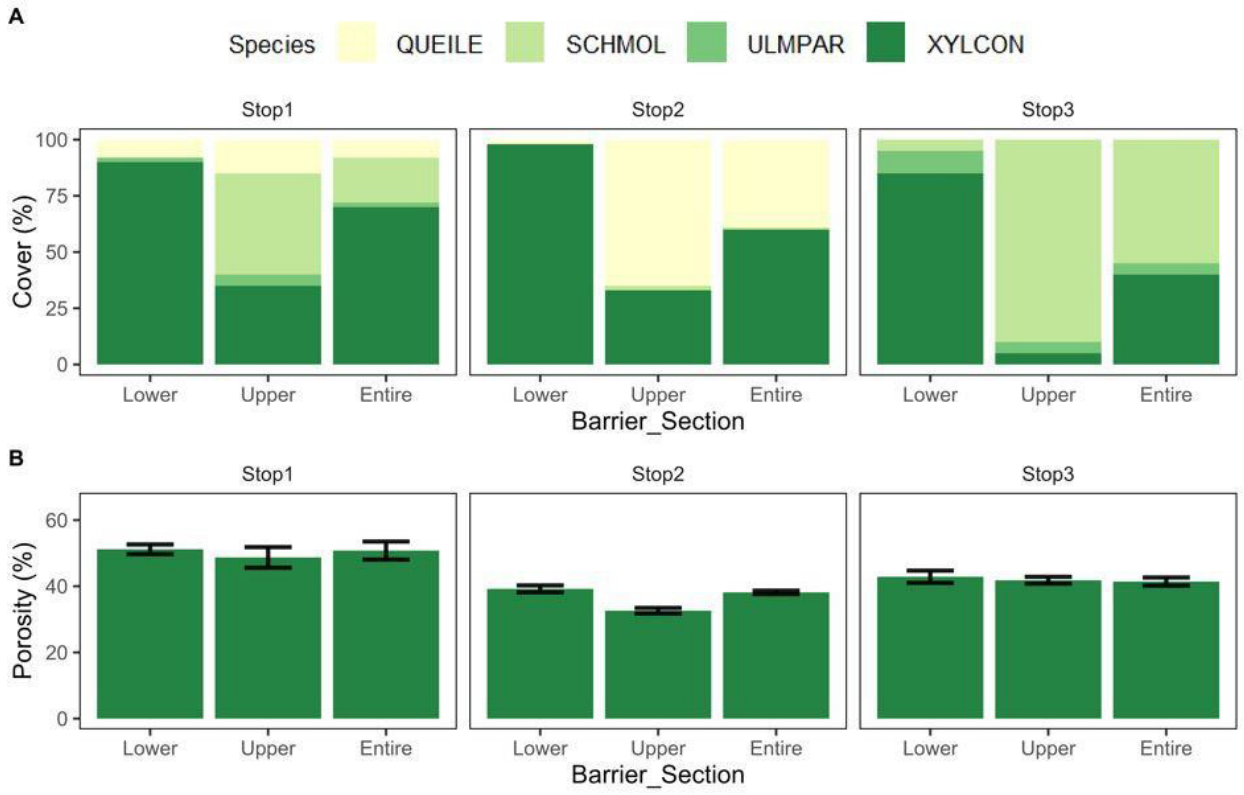


**Figure 4.11.** *Species composition (A) and porosity (B) of vertical profile of three sampling locations from Fall 2025 along the SR-55 vegetation barrier. The barrier is composed of four distinct species: QUEILE – Quercus ilex, SCHMOL – Schinus molle, ULMPAR – Ulmus parviflora, XYLCON – Xylosma congestum. Porosity shows means ± 1SE for the 9 m section of the vegetation barrier sampled.*

## 4.5 Vegetation Characterization

Given the effect that plant species can have a significant effect on the efficacy of a vegetative barrier, an additional assessment of vegetative attributes was undertaken. A focal list of species was compiled based on a suite of conditions:

- The species was identified as having traits that overlap with desired barrier characteristics such as low branching and high foliage density
- The species had been used by Caltrans in projects within the Los Angeles and Orange County Districts either based on direct observations on roadways or a compiled species provided by Caltrans

A focal list of 14 plant species was compiled (Table 4.3). For each of these species, Leaf Area Index (LAI), porosity, height, branching architecture, leaf area, leaf mass area, and stomatal density were measured. The number of individuals sampled depending on availability and ranged from three to nine. LAI, porosity and height, and width were measured following methods outlined in Section 4.3.3. Branching architecture provides a metric of how intensely a plant branches. Frequent branching can indicate that a plant can handle low light conditions (Pickett and Kempf 1980) and may result in higher leaf density. Branching architecture was estimated as the apical dominance index (ADI) following methods outlined by Pérez-Harguindeguy et al. 2013. ADI is the number of ramifications points that lead to living branches divided by the total length of the branch, measured in meters. Three leaves were sampled from each individual to estimate leaf area ($cm^2$) and leaf dry mass (g). Leaf area was estimated from a scanned image of a leaf using ImageJ. Leaf mass area was calculated as the dry mass of the leaf divided by the leaf area. This metric is particularly useful as it allows for the conversion of biogenic emissions between $\mu g\ g^{-1}\ h^{-1}$ and $nmol\ m^{-2}\ s^{-1}$. Stomatal density is an estimate of the number of stomata per a given area of the leaf and was included as this characteristic has been linked to increase particulate matter capture in other studies (Corada et al. 2021; Sgrigna et al. 2020). Stomatal density was measured by applying a layer of clear nail polish on the lower side of the leaf. Once the nail polish is dry a piece of transparent tape is placed on the treated area. After gently peeling the tape, the tape is adhered to a microscope slide to count the number of stomata at 40x magnification (Figure 4.12).

**Table 4.3.** *List of the 14 species surveyed in the additional characterization of roadside vegetation. * Indicates that a species is native to California*

| Species Name | Common Name | Number of Caltrans Projects | Locations Sampled | Number of Individuals Sampled |
|---|---|---|---|---|
| ***Calocedrus decurrens**** | incense cedar | 1 | 33°48'29"N 116°46'37"W<br>33°58'16"N 117°19'11"W<br>33°58'16"N 117°19'10"W | 4 |
| ***Cupressus sempervirens*** | Mediterranean cypress | 1 | 33°58'25"N 117°19'25"W<br>33°58'24"N 117°19'25"W<br>33°58'24"N 117°19'25"W | 3 |
| ***Elaeagnus pungens*** | Thorny Olive | 1 | 33°58'10"N 117°19'36"W<br>33°58'18"N 117°19'35"W<br>33°58'18"N 117°19'35"W | 3 |
| ***Heteromeles arbutifolia**** | Toyon | 7 | 33°27'02"N 117°38'27"W<br>33°27'02"N 117°38'27"W<br>33°27'01"N 117°38'26"W | 3 |
| ***Malosma laurina**** | Laurel Sumac | 6 | 33°31'05"N 117°35'50"W<br>33°31'05"N 117°35'51"W<br>34°07'43"N 117°41'12"W | 3 |
| ***Melaleuca citrina (Callistemon citrinus)*** | Red/Crimson Bottlebrush | 6 | 34°01'41"N 117°43'07"W<br>34°01'41"N 117°43'06"W<br>34°01'41"N 117°43'06"W | 3 |
| ***Nerium oleander*** | Nerium | 5 | 33°54'14"N 118°11'05"W<br>33°54'14"N 118°11'04"W<br>34°03'53"N 117°48'30"W<br>34°03'53"N 117°48'31"W<br>34°03'53"N 117°48'31"W | 5 |

| | | | | |
|---|---|---|---|---|
| ***Pittosporum crassifolium*** | Karo | 5 | 33°58'23"N 117°19'33"W<br>33°58'23"N 117°19'32"W<br>33°58'23"N 117°19'33"W | 3 |
| ***Rhaphiolepis indica*** | Indian Hawthorn | 14 | 33°58'07"N 117°19'37"W<br>33°58'07"N 117°19'39"W<br>33°58'08"N 117°19'39"W | 3 |
| ***Rhus integrifolia**** | Lemonade Berry | 10 | 33°26'06"N 117°37'01"W<br>33°28'06"N 117°40'24"W | 3 |
| ***Rhus ovata**** | Sugar Bush | 10 | 34°07'21"N 117°41'39"W<br>34°07'21"N 117°41'39"W<br>34°07'21"N 117°41'39"W | 3 |
| ***Thevetia peruviana*** | Cascabela thevetia | 13 | 33°29'24"N 117°39'48"W<br>33°29'24"N 117°39'48"W<br>33°29'24"N 117°39'48"W<br>34°07'09"N 117°48'21"W<br>33°59'49"N 117°55'46"W<br>33°59'49"N 117°55'45"W<br>33°59'49"N 117°55'46"W<br>33°54'25"N 118°10'57"W<br>33°54'26"N 118°10'57"W | 9 |
| ***Westringia fruticosa*** | Coastal Rosemary | 4 | 33°26'29"N 117°37'37"W<br>33°26'28"N 117°37'37"W<br>33°26'30"N 117°37'39"W | 3 |
| ***Xylosma congestum*** | Shiny Xylosoma | 6 | 34°04'21"N 117°55'14"W<br>34°04'21"N 117°55'13"W<br>34°04'21"N 117°55'16"W<br>34°01'51"N 118°01'49"W<br>34°01'51"N 118°01'49"W | 5 |

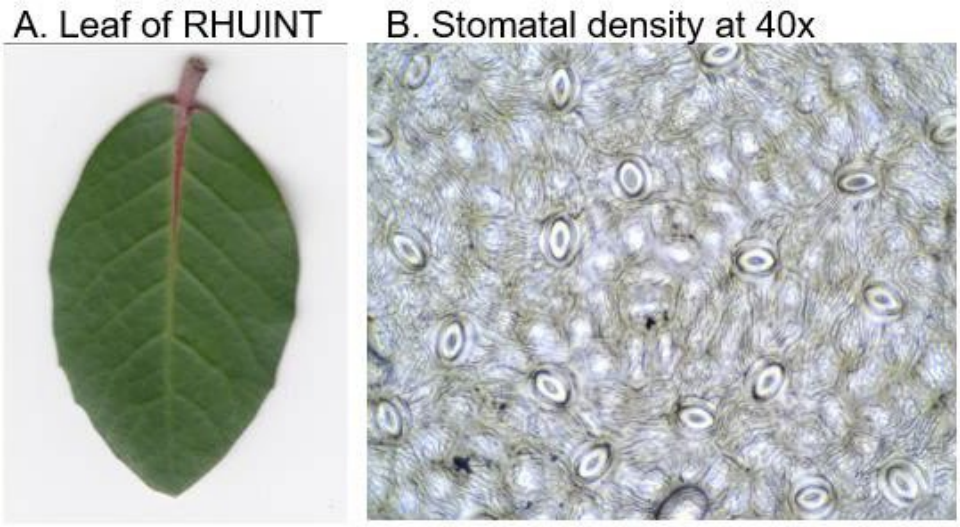


**Figure 4.12.** *A. Leaf scan of Rhus integrifolia (RHUINT) and B. image of stomatal density*

### 4.5.1 Summary of Vegetative Attributes

Height varied across species, ranging from 1.18 m to 13.61 m (Table 4.4). The average height of a species was strongly correlated to plant width, where taller plants were also wider (Figure 4.13). LAI and porosity were also strongly negatively correlated as would be expected where low foliage density likely results in more light traveling through the canopy. Stomatal density showed associations with multiple attributes: positive associations with branching architecture, LAI and negative associations with porosity, leaf area, and leaf mass area. Stomatal density was not measured on 5 species as the position of the stomata required measurement with a scanning electron microscope.

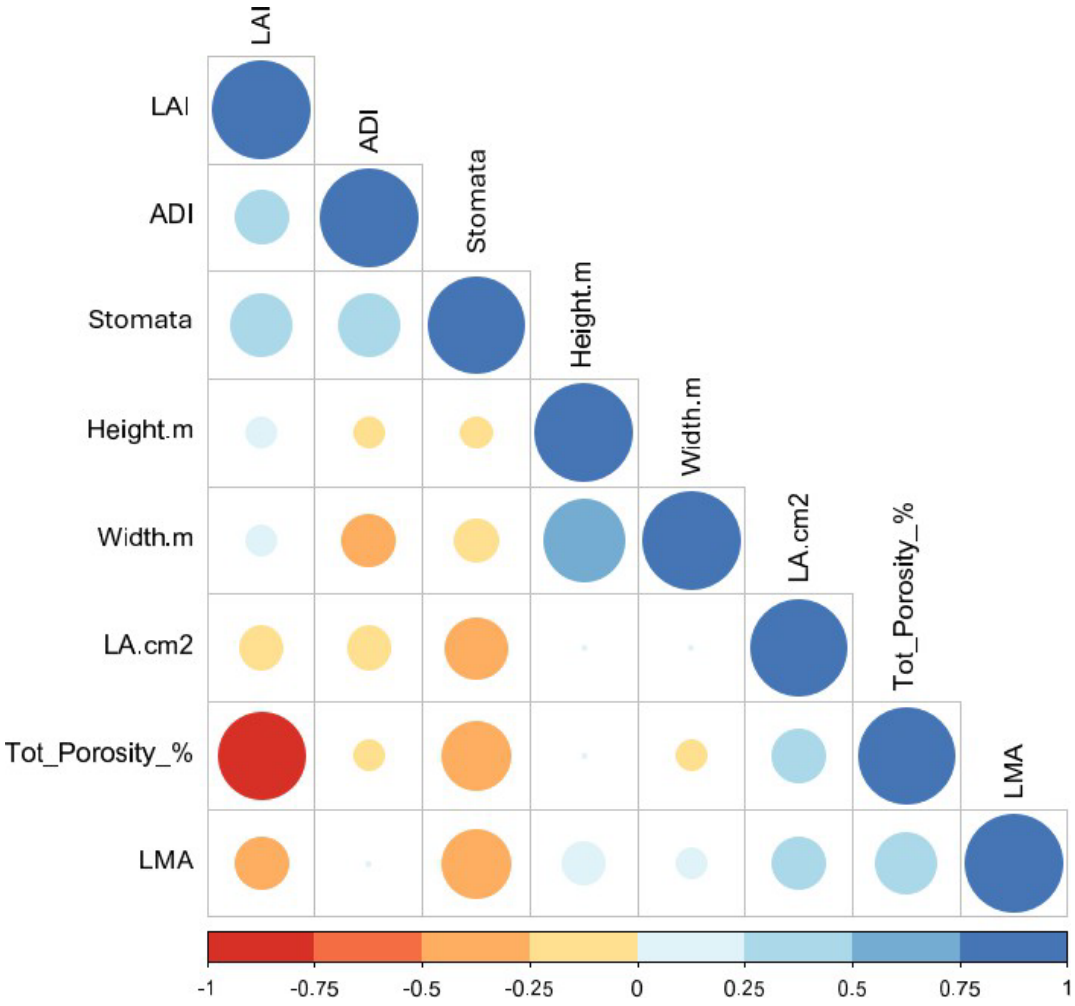


**Figure 4.13.** *Correlation plot of the eight vegetative traits measured on nine roadside plant species. The colors indicate the direction of the correlation with red indicating the two traits are negatively correlated and blue indicating the traits are positively correlated. The size of the circle indicates the strength of the correlation.*

**Table 4.4.** *Average values of the eight vegetative traits measured for the focal species.*

| Species Name | Vegetation Category | Height (m) | Width (m) | LAI | Branching (ADI) | Porosity (%) | Leaf Area ($cm^2$) | LMA ($g/m^2$) | Stomatal Density |
|---|---|---|---|---|---|---|---|---|---|
| **Calocedrus decurrens** | Needleleaf Trees | 11.96 | 7.15 | 0.94 | 45.25 | 47.59 | 0.09 | 255.88 | |
| **Cupressus sempervirens** | Needleleaf Trees | 13.61 | 1.09 | 8.35 | 111.55 | 10.17 | 0.13 | 305.99 | |
| **Elaeagnus pungens** | Shrub | 1.46 | 1.88 | 0.81 | 9.14 | 32.56 | 28.87 | 99.22 | |
| **Heteromeles arbutifolia** | Shrub | 2.55 | 2.85 | 3.03 | 22.34 | 29.71 | 17.91 | 176.31 | 133.29 |
| **Malosma laurina** | Temperate Broadleaf Trees | 3.98 | 4.97 | 2.88 | 9.29 | 28.61 | 31.61 | 185.46 | 98.21 |
| **Melaleuca citrina** | Shrub | 3.48 | 3.23 | 5.77 | 19.95 | 18.32 | 12.48 | 171.76 | 157.14 |
| **Nerium oleander** | Shrub | 1.89 | 3.19 | 1.40 | 10.56 | 32.46 | 15.41 | 173.70 | |
| **Pittosporum crassifolium** | Shrub | 1.87 | 3.23 | 7.85 | 11.77 | 6.77 | 24.98 | 114.43 | 143.11 |
| **Rhaphiolepis indica** | Shrub | 1.18 | 2.62 | 2.84 | 16.92 | 21.31 | 21.42 | 194.87 | 204.84 |
| **Rhus integrifolia** | Shrub | 3.17 | 4.29 | 2.89 | 12.56 | 26.52 | 13.34 | 230.81 | 137.50 |
| **Rhus ovata** | Shrub | 3.20 | 5.50 | 4.21 | 6.56 | 16.69 | 23.46 | 280.58 | 72.96 |

| | | | | | | | | | |
|---|---|---|---|---|---|---|---|---|---|
| **Thevetia peruviana** | Shrub | 2.70 | 4.40 | 3.89 | 9.50 | 15.07 | 9.75 | 81.57 | 199.23 |
| **Westringia fruticosa** | Shrub | 2.12 | 3.14 | 10.93 | 55.57 | 0.20 | 0.50 | 147.90 | |
| **Xylosma congestum** | Shrub | 3.20 | 3.95 | 6.47 | 19.66 | 8.40 | 16.42 | 108.90 | 321.57 |

Of the 14 species, nine species have measured biogenic emissions. Four of the species - *Nerium oleander*, *Rhaphiolepis indica*, *Rhus ovata*, *Thevetia peruviana* – were reported as below detection level (Benjamin and Winer 1998; Padhy Varshney et al 2005). One species was classified as a medium emitter by Caltrans – *Melaleuca citrina* due to its isoprene emissions (Benjamin and Winer 1998; Caltrans 2024). The other four species *Calocedrus decurrens*, *Cupressus sempervirens*, *Heteromeles arbutifolia*, and *Xylosma congestum* are designated as low emitters (Benjamin and Winer 1998, Nagalingam et al. 2024). *Elaeagnus pungens*, *Malosma laurina*, *Pittosporum crassifolium, Rhus integrifolia*, and *Westringia fruticosa* do not have published emission data.

### 4.5.2 Estimating Deposition Velocities of Particulate Matter

We conducted several experiments to estimate the deposition velocity of PM10 by using an opening on the solid barrier next to Highway I-215, adjacent to Parking Lot 6. The opening served as a natural wind tunnel. The goal of this experiment was to assess the potential of tree leaves to capture airborne roadway dust. To model leaf surfaces, sheets of cardboard were prepared with adhesive tape to simulate the sticky surface characteristics of foliage.

Multiple cardboard collectors were assembled and placed in different orientations to evaluate how configuration influences dust deposition. The placements included:

- One horizontal surface positioned near the bottom of the opening.
- One vertical surface for impaction
- Two horizontal surfaces positioned mid-height
- Two vertical edge-oriented surfaces placed mid-height
- Two additional surfaces oriented for impaction

To quantify pollutant gradients, two PurpleAir sensors and two black carbon (BC) monitors were installed to measure upwind and downwind concentrations relative to the highway. A 3-D sonic anemometer was positioned downwind to record wind speed and direction.

Photographs of the instrument placements and experimental configurations are shown in Figure 4.14.

**Figure 4.14.** *Set up Deposition Experiments*

The data from these experiments yielded deposition velocities in excess of 10 cm/s for PM10, which are well above deposition velocities reported in the literature. These results appeared to be related to the deposition of large particles of particulate matter on the cardboard surfaces. We did not find a way of removing these particles from the surfaces without disturbing the deposited material on the surface. In view of this, we recommend applying VBM using estimates from comprehensive models of deposition velocities or measured values reported in the literature (Farmer et al., 2021).

## 4.6 References


- Baldauf, R. (2017). Roadside vegetation design characteristics that can improve local, near-road air quality. *Transportation Research Part D: Transport and Environment*, 52, 354–361. https://doi.org/10.1016/j.trd.2017.03.013
- Benjamin, M.T. and Winer, A.M. (1998). Estimating the ozone-forming potential of urban trees and shrubs. Atmospheric Environment 32:53-68
- California Department of Transportation. (2024). Volatile Organic Compound Emissions from Plant Species Used by Caltrans and an Analysis of Their Potential Air Quality Impacts. CTAQ-TM-24-435.03.03
- Dunn, G.M. and Martin, S.R. (2004), Yield prediction from digital image analysis: A technique with potential for vineyard assessments prior to harvest. Australian Journal of Grape and Wine Research, 10: 196-198. https://doi.org/10.1111/j.1755-0238.2004.tb00022.x
- Farmer, D.K., Boedicker, E.K., Debolt, H.M., 2021. Dry Deposition of Atmospheric Aerosols : Approaches , Observations , and Mechanisms.
- Nagalingam, S., Wang, H., Kim, S., and Guenther, A. (2024). Unexpectedly strong heat stress induction of monoterpene, methylbutenol, and other volatile emissions for conifers in the cypress family (Cupressaceae). Science of The Total Environment 956:177336
- Padhy, P.K. and Varshney, C.K. 2005. Emission of volatile organic compounds (VOC) from tropical plant species in India. Chemosphere 59:1643-1653
- Pérez-Harguindeguy N., Díaz S., Garnier E., Lavorel S., Poorter H., Jaureguiberry P., Bret-Harte M. S., Cornwell W. K., Craine J. M., Gurvich D. E., Urcelay C., Veneklaas E. J., Reich P. B., Poorter L., Wright I. J., Ray P., Enrico L., Pausas J. G., de Vos A. C., Buchmann N., Funes G., Quétier F., Hodgson J. G., Thompson K., Morgan H. D., ter Steege H., van der Heijden M. G. A., Sack L., Blonder B., Poschlod P., Vaieretti M. V., Conti G., Staver A. C., Aquino S., Cornelissen J. H. C. (2013) New handbook for standardised measurement of plant functional traits worldwide. Australian Journal of Botany 61, 167–234.

- Pickett STA, Kempf JS (1980) Branching patterns in forest shrubs and understory trees in relation to habitat. New Phytologist 86, 219–228.
- Sgrigna, G., Baldacchini, C., Dreveck, S., Cheng, Z., & Calfapietra, C. (2020). Relationships between air particulate matter capture efficiency and leaf traits in twelve tree species from an Italian urban-industrial environment. *Science of the Total Environment*, *718*, 137310.

# Chapter 5

## Evaluation of Model

## 5.1 Introduction

In Chapter 2, we proposed the model

$$C_v = (1-\varepsilon)C_b + \varepsilon C_f \alpha_t f_d \tag{5.1}$$

where $C_v$ is the concentration downwind of the vegetative barrier, $C_b$ is the concentration at the same location downwind of a solid barrier with the same height as the vegetative barrier, and $C_f$ is the corresponding concentration in the absence of a barrier. So $C_v$ interpolates between the two possible limits of the concentration using the optical porosity, $\epsilon$, (Raupach et al., 2001) as the interpolating parameter.

The first term on the right-hand side of Equation (5.1) says that the flow that does not go through the barrier behaves as if it encounters a solid barrier, and the dispersion is governed by the model for sold barriers. The second term on the right says that the flow that goes through the barrier behaves like one in the absence of a barrier. The factor, $f_d$, accounts for dry deposition/impaction of pollutants in the barrier, and $\alpha_t$ accounts for the effects of the vegetation on turbulence.

It is difficult to evaluate the model directly by comparing model results with corresponding observations because the emission rate from the road is uncertain and the contribution of the road to the measured concentrations is relatively small relative to background concentrations typical of southern California. To overcome this problem, we developed an indirect approach to model evaluation that took advantage of the empirical relationship among the PM concentrations measured at the three sites next to SR-55: downwind of the vegetative barrier, downwind of the solid barrier, and open area.

We found that the three sets of concentrations were related to each other through

$$C^m_{VB} = (1-w)C^m_{SB} + wC^m_{OA} \tag{5.2}$$

where the $C^m_{VB}$ is the concentration measured downwind of the vegetative barrier, (VB), $C^m_{SB}$ is the concentration downwind of the downwind of the solid barrier (VB), and $C^m_{OA}$ is the concentration measured in the open area. We see that this equation also applies to the contribution of emissions from the road by subtracting a constant background from each of the concentrations. We can write

$$\frac{C^p_{VB}}{Q} = (1-w)\frac{C^p_{SB}}{Q} + w\frac{C^p_{OA}}{Q} \tag{5.3}$$

where $Q$ is the unknown highway emission rate, and the superscript '$p$' denotes model estimate. We can now evaluate the model for the vegetation barrier by testing whether the weight, $w$, derived from the data also applies to modeled $C/Q$, which does not require knowledge of the emission rate. We assume that we can model $C^p_{SB}/Q$ and $C^p_{OA}/Q$ using equations that have been evaluated in previous studies (Thiruvenkatachari et al., 2022;Snyder et al., 2013).

The model for the vegetative barrier, $C^p_{VB}/Q$, assumes that optical porosity, $\epsilon$, is the dominant factor in determining concentrations so that

$$C^p_{VB} = (1-\varepsilon)C^{pV}_{SB} + \varepsilon C^{pV}_{OA} \tag{5.4}$$

where the superscript '$pV$'implies that the computed concentrations correspond to the locations of the vegetative barrier and the associated meteorology and associated receptors. The parameter, $'\epsilon'$, in the equation is the value that best fits Equation (5.4) using the same weighting factor as that obtained from equation (5.3) fitted to measurements. The adequacy of the model is determined by the quality of the explanation provided by Equation (5.4), and the agreement between the implied value of $\epsilon$ and the measured value.

## 5.2 Analysis of Data from the SR-55 Field Study

We first show the analysis of data collected on 9/23/2025, in Figure 5.1, when there was a significant range of the concentrations measured collected over four hours. The relationship among measurements, described by Equation (5.3) is mimicked well by the corresponding modeling values when the inferred porosity is 0.53. Note that the weight of 0.46 inferred from measurements is also used to combine modeled PM values downwind of the solid barrier and the open area. The inferred value of porosity is consistent with measurements of porosity, described in Chapter 4.

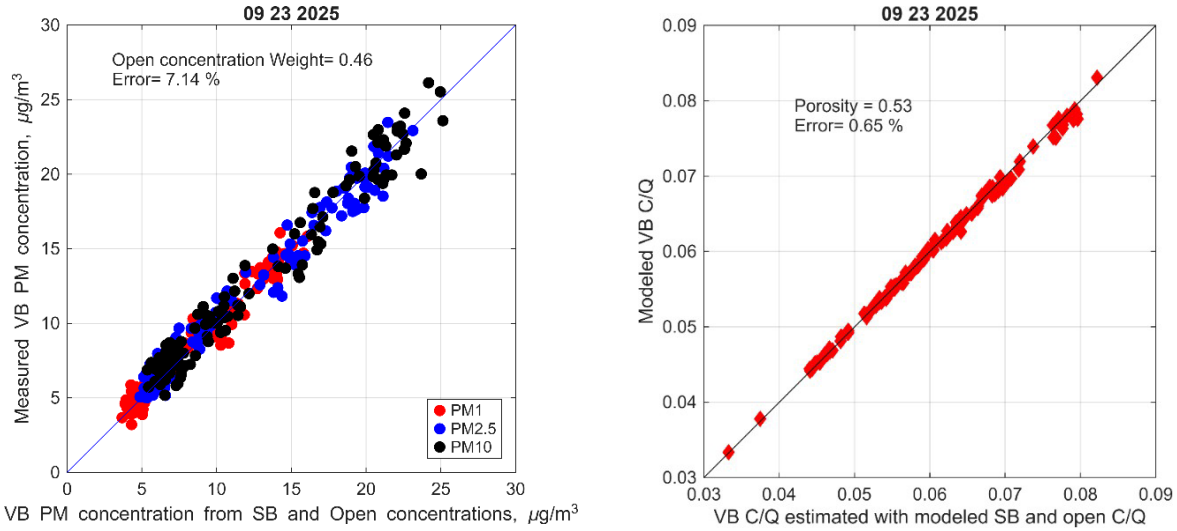


**Figure 5.1.** *PM concentrations downwind of the open area and solid barrier fitted to concentrations measured downwind of vegetative barrier. Left panel shows measured values and right panel shows corresponding modeled values fitted with the weight used for measurements.*

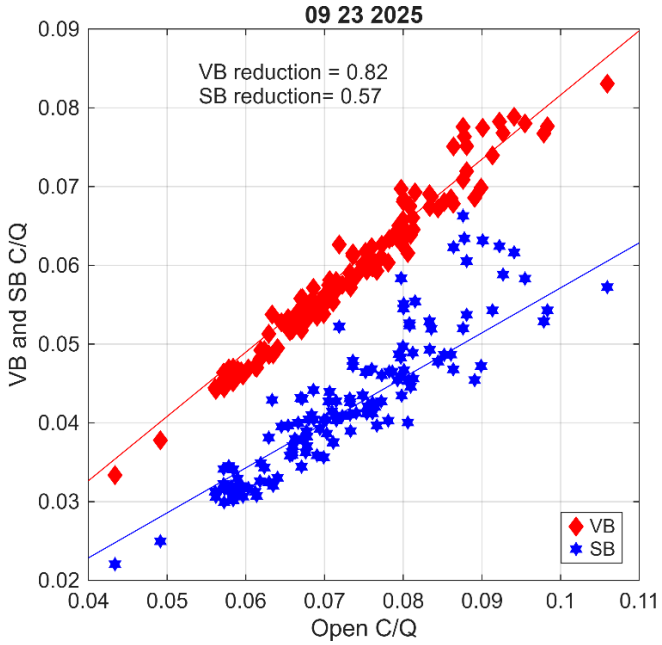


**Figure 5.2.** *Modeled impacts of vegetative and solid barriers on downwind concentrations relative to open area.*

Figure 5.2 shows the modeled impacts of the vegetative and solid barriers relative to an open area at the receptors downwind of the vegetative barrier. For this particular case, the vegetative barrier

is $\frac{0.57}{0.82} = 70\%$ as efficient as the solid barrier in reducing concentrations at receptors 2-5 m downwind of the barriers. As seen in Chapter 2, both downwind barrier concentrations approach that of the open area at about 50 times the barrier height.

The performance of the vegetative barrier in describing observations varies with the field study day. Figure 5.3 shows a case in which the measured concentrations show good agreement with Equation (5.3), while the modeled values show considerable scatter about the one-to-one line. At this point we are unable to provide a possible explanation for the larger scatter on 5/31 relative to that on 9/23.

Figure 5.4 shows the concentration reductions associated with the vegetative and solid barriers. In this case, the vegetative barrier is about 80% as effective as the solid barrier in reducing concentrations just downwind of the barrier.

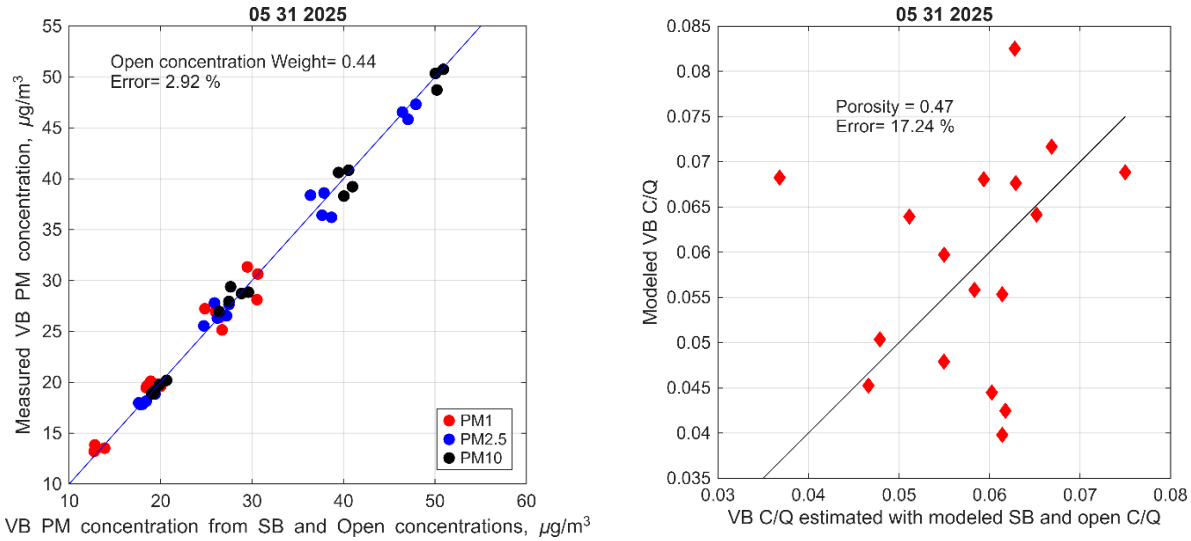


**Figure 5.3.** *PM concentrations downwind of the open area and solid barrier fitted to concentrations measured downwind of vegetative barrier. Left panel shows measured values and right panel shows corresponding modeled values fitted with the weight used for measurements.*

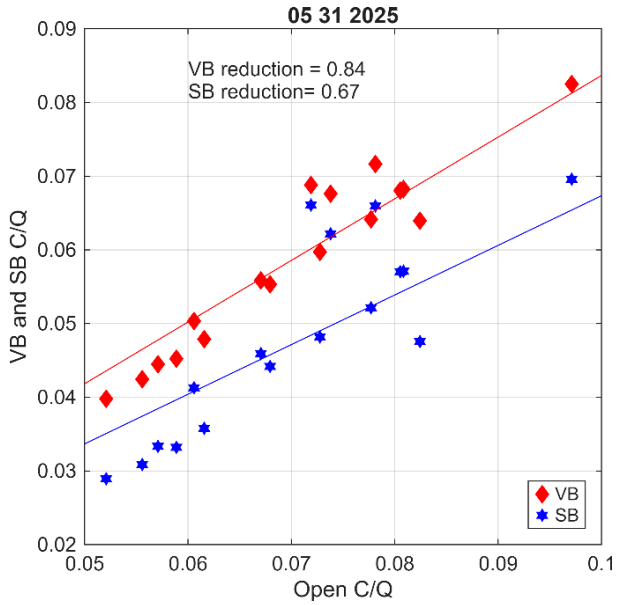


**Figure 5.4.** *Modeled impacts of vegetative and solid barriers on downwind concentrations relative to open area.*

Table 5.1 shows the data that are collected in field studies on SR-55 for dates of 11/04/2023, 01/15/2024, 05/31/2025, 09/22/2025, 09/23/2025 and 09/25/2025 porosity of the vegetation barrier, reduction after the vegetation and solid barrier and the fitting error percentage for measurement and model.

**Table 5.1.** *Results of Data collected in Field Studies at SR-55*

| Date | Measurement Fitting Error % | Model Fitting Error % | Porosity | VB Reduction | SB Reduction | No of Points |
|---|---|---|---|---|---|---|
| **05 31 2025** | 2.92 | 17.24 | 0.47 | 0.84 | 0.67 | 17 |
| **09 22 2025** | 7.45 | 0.68 | 0.65 | 0.86 | 0.57 | 57 |
| **09 23 2025** | 7.14 | 0.65 | 0.53 | 0.82 | 0.57 | 131 |
| **09 25 2025** | 10.34 | 0.51 | 0.57 | 0.82 | 0.57 | 80 |

| Date | Measurement Fitting Error % | Model Fitting Error % | Porosity | VB Reduction | SB Reduction | No of Points |
|---|---|---|---|---|---|---|
| **09 22 2025** | 7.30 | 22.54 | 0.65 | 0.86 | 0.55 | 10 |
| **09 23 2025** | 6.26 | 11.51 | 0.57 | 0.82 | 0.55 | 20 |
| **09 25 2025** | 4.23 | 13.45 | 0.67 | 0.86 | 0.55 | 17 |
| **01 15 2024** | 3.55 | 0.99 | 0.69 | 0.90 | 0.61 | 85 |
| **11 04 2023** | 4.04 | 0.69 | 0.51 | 0.78 | 0.53 | 6 |

The next section describes the evaluation of the vegetation barrier model using data from a field study conducted in Woodside, California.

## 5.3 Evaluation of Data from Woodside Study

Recall from Chapter 4 that stationary measurements of pollutant concentrations were made at the Stops shown in Figure 5.5. The characteristics of the vegetation at each Stop are listed in Table 5.2.

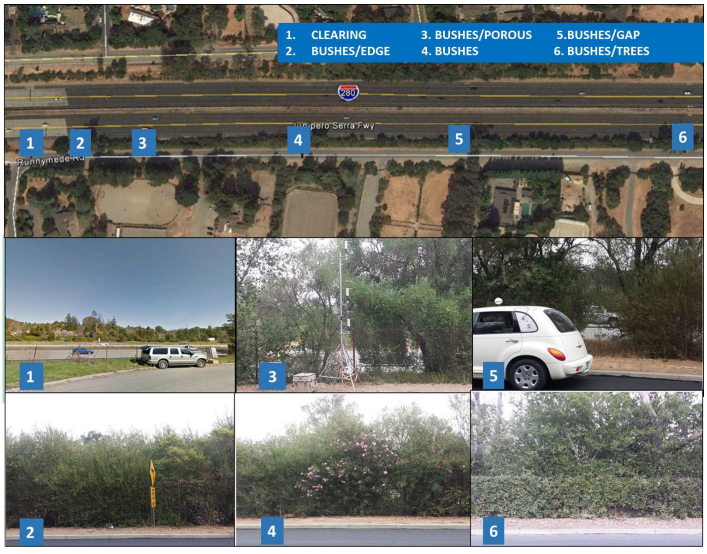


**Figure 5.5.** *Aerial view of the study location including Interstate-280, the parallel access road, and the neighborhood to the south of the highway. The inserts at the bottom show a view of the vegetation characteristics at each measurement location, which correspond to the estimates of vegetation porosity at each location as listed in Table 5.2.*

**Table 5.2.** *Characteristics of Sites sampled at Woodside, California*

| Stop | Descriptor | Height(m) | Width(m) | Porosity* | Notes |
|---|---|---|---|---|---|
| **1** | CLEARING | <1 | <1 | 100 | Grass and low bushes only; no obstruction to air flow |
| **2** | BUSHES/EDGE | 3 | 5 | 25 | Bushes only; located approximately 20m from clearing |
| **3** | BUSHES/POROUS | 5 | 5 | 50 | Porous vegetation with bushes and trees, including large gaps with limited or no vegetation |
| **4** | BUSHES | 4 | 10 | 10 | Mix of thick bushes and flowering oleanders |
| **5** | BUSHES/GAP | 5 | 10 | 25/90 | Bushes (25% porosity) on either side of an approximately 1.5m wide, gap (90% porosity) |
| **6** | BUSHES/TREES | 10 | 10 | 10 | Mix of bushes approximately 2m tall with trees extending above to approximately 10m |

* Porosity estimated visually from pictures as shown in Figure 5.5.

As indicated in the previous section, measurements of the concentrations of CO, $NO_2$, black carbon, ultrafine particles were made by parking the mobile platform for ten minutes at each Stop, after which the platform made a loop using the highway; about 5 to 7 loops were made each day. The results presented in Deshmukh et al., ( 2019) show that these pollutants show differing concentration reductions relative to Stop 1. The paper provides some reasons for this behavior. Here, we examine the "average" reductions by normalizing the pollutants by their means and treating all the species as one pollutant. Because the concentrations were measured during time intervals, it was not possible to pair them in time to compute the concentration reductions relative to the concentrations measured in the open area. So, we compared the distributions of the measured concentrations through 10 equally points between the $25^{th}$ and the $95^{th}$ percentiles of the distributions; these points served as pseudo concentrations that were paired with corresponding points in distribution of concentrations at other Stops. This approach assumes that high and low concentrations at the Stops would be correlated if the concentrations were measured simultaneously behind the different vegetative barriers. We expect the results to reflect the uncertainty associated with the differences in meteorology and highway emissions during the time intervals being compared.

Reductions in concentration were computed by considering wind directions within $90^0$ of the normal to the road. Model estimates were also computed for this wind direction interval. Figure 5.6 shows the concentration reductions at the different Stops as a function of concentration corresponding to the 10 equally spaced percentiles between the $25^{th}$ and $95^{th}$ percentiles. We see that the mitigating impact of the vegetative barrier ranges from about 5% to 20% relative to the open section. The modeling, described next, indicates that the negative reductions at Stop 3 are related to the difference in meteorology in the sampling intervals used at Stop 3 and Stop 1, the open section; it does not imply a concentration increase induced by the vegetative barrier.

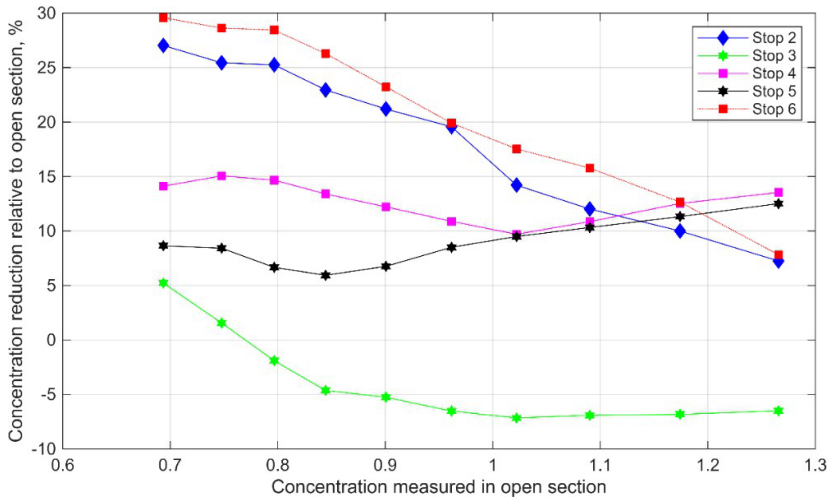


**Figure 5.6.** *Concentration distributions at Stops. Each point on the line is the concentration on the cumulative distributed of the concentrations measured at the Stop. The minimum concentration along each line corresponds to the 25th percentile and the maximum concentration to the 95th percentile.*

Figure 5.7 presents the modeled mean reductions compared to the measured values. The porosities are values corresponding to the best agreement between the measured and modeled mean concentration reductions. We see that the visually determined porosities, presented in Table 5.3, differ from the inferred values shown in the Figure 5.5. At Stop 2, there is little disagreement between the two values. At Stop 3, the modeled value indicates that the vegetative barrier offers little resistance to flow through it; the increase in concentration is caused by the difference in meteorology between Stop 1 and Stop 3. The experimental value at Stop 3 is 50%. The inferred porosities at Stop 4 and 6 are much higher than the visually determined values. At Stop 5, the inferred value of 48% is within the visually suggested range of 25 to 90%.

**Table 5.3.** *Comparison of "Visual" with Model-Inferred Porosities.*

| Stop Number | Visually determined porosity (%) | Inferred porosity (%) |
|---|---|---|
| **2** | 25 | 27 |
| **3** | 50 | 97 |
| **4** | 10 | 59 |
| **5** | 25/90 | 48 |
| **6** | 10 | 58 |

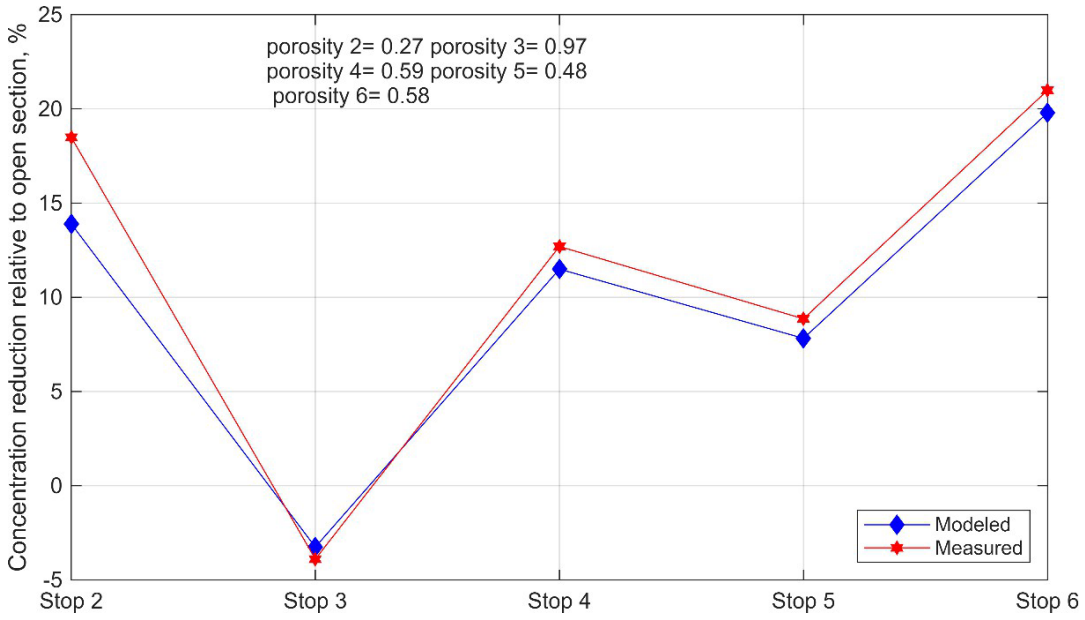


**Figure 5.7.** *The mean reductions at each stop are relative to the concentration at Stop 1, the open section without a barrier. The porosities correspond to the values that provide the best fit between the mean measured and modeled reductions at each Stop.*

## 5.4 Analysis of Results from Sacramento Study

The field study was conducted in Sacramento, California, next to CA-99 in Sacramento. The freeway, which has an average traffic flow rate of 200,000 vehicles/day, is 42 m wide and has 10 lanes including 2 High Occupancy Vehicle (HOV) lanes. The barrier is 12 m from the edge of the highway, which is the only major source of pollution near the study area. The primary objective of the study was to examine the effect of tall vegetation behind a barrier on concentration levels in the vicinity of the highway.

A re-examination of the data did not provide any quantitative information that could be used in formulating VBM. The primary qualitative conclusion is that on average, the concentration levels behind the vegetation-wall barrier are 0.87 of the corresponding values behind the wall. Although the vegetation enhances the mitigation effect of the solid barrier, this is not the case for all of the observed data. This result is illustrated in Figure 5.8, which shows the time series of 1-min averaged UFP concentrations during June 25$^{th}$ and 26$^{th}$, 2016, of the sampling campaign. The background concentrations do not vary significantly and they are of the order of 5000 #/cm$^3$, which indicates that freeway emissions have minor impact on the upwind receptor. On the other hand, the downwind UFP concentrations at both sites show significant variations, with spikes reaching $6 \times 10^4$ #/cm$^3$.

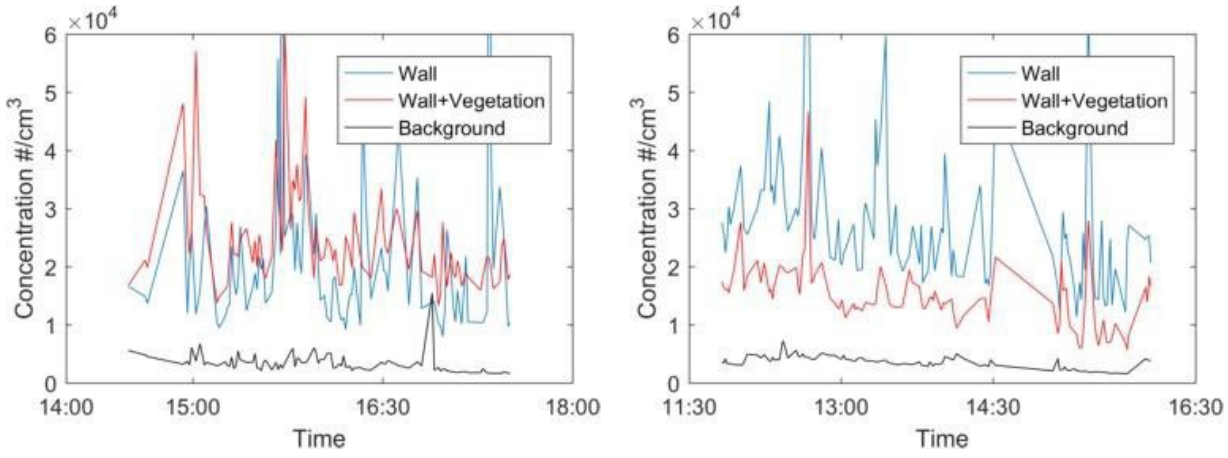


**Figure 5.8.** *Time series of 1-min averaged ultrafine concentrations during a) June 25th and b) June 26th, 2016.*

These results suggest accounting for the effects of a vegetative barrier behind a wall by increasing the effective height of the solid barrier and decreasing the entrainment of material into the wake of the solid barrier. The data from the field study did not provide information that can be used to make quantitative modifications to VBM.

## 5.5 References


- Deshmukh, Parikshit, Vlad Isakov, Akula Venkatram, Bo Yang, K. Max Zhang, Russell Logan, and Richard Baldauf. 2019. "The Effects of Roadside Vegetation Characteristics on Local, near-Road Air Quality." *Air Quality, Atmosphere and Health*. https://doi.org/10.1007/s11869-018-0651-8.
- Raupach, M. R., N. Woods, G. Dorr, J. F. Leys, and H. A. Cleugh. 2001. "The Entrapment of Particles by Windbreaks." *Atmospheric Environment*.
- Snyder, Michelle G, Akula Venkatram, David K Heist, Steven G Perry, William B Petersen, and Vlad Isakov. 2013. "RLINE: A Line Source Dispersion Model for near-Surface Releases." *ATMOSPHERIC ENVIRONMENT* 77 (October): 748–56. https://doi.org/10.1016/j.atmosenv.2013.05.074.
- Thiruvenkatachari, Ranga Rajan, Yifan Ding, David Pankratz, and Akula Venkatram. 2022. "A Field Study to Estimate the Impact of Noise Barriers on Mitigation of near Road Air Pollution." *Air Quality, Atmosphere and Health* 15 (2): 363–72. https://doi.org/10.1007/s11869-021-01104-9.

# Chapter 6

## Vegetative Barrier Model

## 6.1 Introduction

The Vegetative Barrier Model consists of two sub-models: Dispersion Model (DM), and VOC Emission Model (VEM). The DM estimates particulate matter concentrations at specified receptors, while the VEM estimates emission rates of biogenic volatile organic compounds from the specified vegetative barrier. The formulation of the DM is described in Chapter 3, and its evaluation is described in Chapter 4. The VEM is based on the MEGAN (*Model of Emissions of Gases and Aerosols from Nature*) model. Details of its formulation are described in Guenther et al. (2012).

The next two sections describe the inputs and outputs of the DM and the VEM. They are currently coded in MATLAB. These sub-models are packaged in an executable VBM with an interface that facilitates its application by a non-expert.

## 6.2 Dispersion Model

The Dispersion Model uses 4 input files:

1) Source file that provides the two-dimensional coordinates of the highway, whose impact is being examined. The highway is represented first via a convenient coordinate system that specifies the beginning and end points. Additionally, the segment of highway being studied is described through its *length*, *width*, *number of lanes*, and its orientation with respect to north. The code generates the line sources that constitute the highway. Table 6.1 provides an example of this information in Excel format.

**Table 6.1.** *Source input for Dispersion Model*

| xsb | ysb | xse | yse | Rwidth | Nlanes | RdAngle | zs | xwall |
|---|---|---|---|---|---|---|---|---|
| **0** | 0 | 0 | 300 | 40 | 4 | -20 | 1 | 10 |

In Table 6.1, (**xsb, ysb**) denotes the beginning of the line representing the edge of the highway, and (**xse, yse**) are the ends of the highway segment whose length is 300 m. The width is 40 m, and there are 4 lanes. The road segment is at an angle of -20 degrees rotated anticlockwise relative to the north direction. The height of emission, **zs**, is specified as 1m, and the distance of the vegetative barrier from the edge of the highway, **xwall**, is 10 m.

2) Receptor File: This specifies the x, y, and z co-ordinates of the receptors relative to the edge of the road in the coordinate system used to specify the road. Table 6.2 provides an example of the file for three receptors.

**Table 6.2.** *Receptor Inputs for Dispersion model*

| xr | yr | zr |
|---|---|---|
| **17** | 100 | 2 |
| **25** | 30 | 2 |
| **30** | 250 | 2 |

Together, the input data can be used to generate Figure 6.1 depicting the road (black lines), the vegetative barrier (green line), and the receptors (red diamonds).

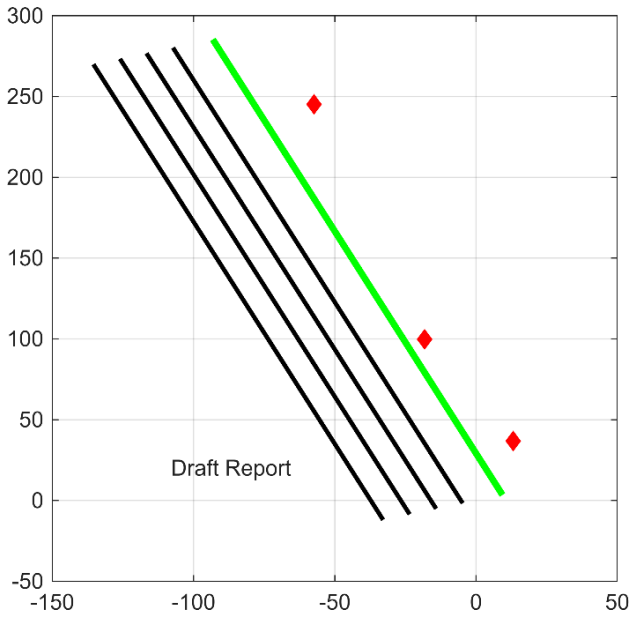


**Figure 6.1.** *The black lines denote the centerlines of the 4 lanes, the green line corresponds to the vegetative barrier, and the red diamonds to the receptors*

3) The vegetative barrier is described through its height, optical porosity, leaf area index, width and deposition velocity, attributes that will impact dispersion of highway emissions. Table 6.3 summarizes these data for the SR-55 vegetation barrier.

**Table 6.3.** *Specification of SR-55 vegetation barrier*

| hwall | por | LAI | vd | width |
|---|---|---|---|---|
| **5** | 0.5 | 5 | 0.01 | 5 |

In Table 6.3, **hwall** is the height of the barrier in meters, **por** is the optical porosity of the barrier, **LAI** is the leaf area index, **vd** is the deposition velocity of PM10 in m/s and **width** is the width of the barrier in meters.

4) Emission file species the traffic flow rate (Traf; veh/h) and the emission factor (EF; g/veh.km) over the period of interest. Table 6.4 shows this information during the first 5 hours of the day.

**Table 6.4.** *Sample Emission Factor and Traffic flow*

| Hour | Traf | EF |
|---|---|---|
| **1** | 5000 | 0.05 |
| **2** | 6000 | 0.05 |
| **3** | 5000 | 0.05 |
| **4** | 6000 | 0.05 |
| **5** | 7000 | 0.05 |

5) Meteorology File is the .sfc file generated by AERMET (AERMOD's meteorological processor) for the hours during which the emissions are specified. Table 6.5 provides a partial .sfc file for 5 hours. The .sfc file does NOT identify meteorological variables in its column headers. The code reads the specified .sfc file, and attaches the variable names, such as friction velocity and Monin-Obukhov length, required by the dispersion model.

**Table 6.5.** Example of .sfc file required by Dispersion Model of VBM

| yy | mm | dd | jday | hr | htflx | ustar | wstar | dtdz | pbl | sbl | MOLength | z0 | Bo | alb | wspd | wdir | zref | tt | tref | RH | PRES | CLDCOV |
|---|---|---|---|---|---|---|---|---|---|---|---|---|---|---|---|---|---|---|---|---|---|---|
| **2025** | 5 | 31 | 151 | 1 | -6.3 | 0.114 | -9 | -9 | -999 | 92 | 20.9 | 0.292 | 2.82 | 1 | 1.08 | 135 | 10.1 | 288.9 | 6.2 | 77 | 1004 | 0 |
| **2025** | 5 | 31 | 151 | 2 | -4.6 | 0.097 | -9 | -9 | -999 | 72 | 17.8 | 0.242 | 2.82 | 1 | 0.97 | 8 | 10.1 | 288.7 | 6.2 | 77 | 1004 | 3 |
| **2025** | 5 | 31 | 151 | 3 | -2.5 | 0.077 | -9 | -9 | -999 | 51 | 16.2 | 0.242 | 2.82 | 1 | 0.67 | 16 | 10.1 | 288.4 | 6.2 | 83 | 1004 | 0 |
| **2025** | 5 | 31 | 151 | 4 | -2 | 0.064 | -9 | -9 | -999 | 39 | 12.2 | 0.215 | 2.82 | 1 | 0.5 | 189.9 | 7.2 | 288.2 | 6.2 | 80 | 1004 | 0 |

The DM uses this input to estimate PM10 concentrations over the time period as shown in Table 6.6, the concentrations at receptor 1 over a 23-hour period, are depicted in Figure 6.2.

**Table 6.6.** PM10 Concentrations in $\mu g/m^3$ estimated by DM at the 3 specified receptors

| Hour | Receptor 1 | Receptor 2 | Receptor 3 |
|---|---|---|---|
| **1** | 3.42 | 3.15 | 3.52 |
| **2** | 4.71 | 4.31 | 4.88 |
| **3** | 4.79 | 4.39 | 4.97 |
| **4** | 3.93 | 3.61 | 4.06 |
| **5** | 4.06 | 3.73 | 4.19 |

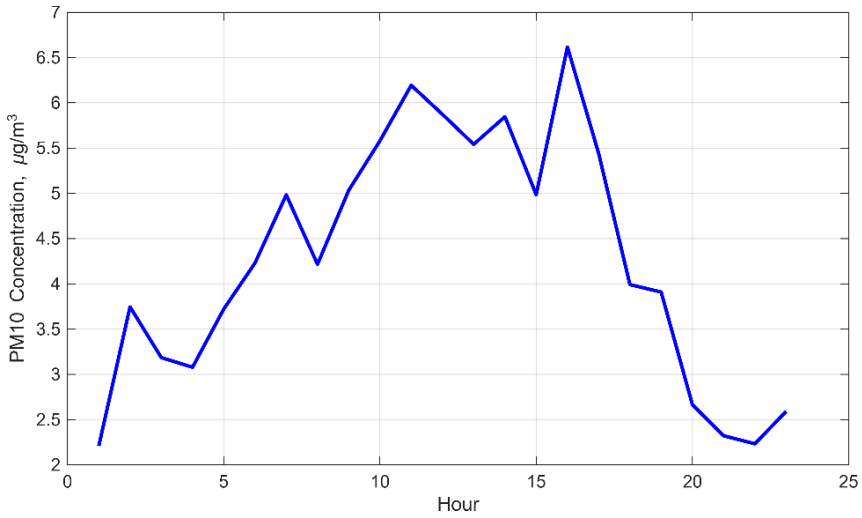


**Figure 6.2.** *Estimates of PM10 concentrations at Receptor 1 produced by the model*

## 6.3 VOC Emission Model

The application of MEGAN requires the mapping of species common in vegetative barriers to plant functional types (PFT), each of which is related to a vector of empirically determined emission rates of several species. The PFT consists of:

- Needleleaf trees
- Tropical trees
- Temperate broadleaf trees
- Shrubs
- Herbaceous species
- Crop

We sampled roadside vegetation at several locations in Southern California, including the SR-55 site, to assign PFTs to the species that we found at these barriers. Table 6.7 summarizes this mapping. If a barrier consists of multiple species that span multiple PFTs, it is necessary to estimate their proportional abundance and sum these abundances across the PFTs.

Table 6.8 provides an example of the PFTs found at three sampling locations along the SR-55 described in Chapter 4. This information is the primary input to MEGAN.

**Table 6.7.** Mapping Species, found in Vegetative Barriers, to MEGAN Plant Functional Type

| Species Name | MEGAN PFT |
|---|---|
| ***Calocedrus decurrens*** | Needleleaf Trees |
| ***Cupressus sempervirens*** | Needleleaf Trees |
| ***Elaeagnus pungens*** | Shrub |
| ***Heteromeles arbutifolia*** | Shrub |
| ***Malosma laurina*** | Temperate Broadleaf Trees |
| ***Melaleuca citrina*** | Shrub |
| ***Nerium oleander*** | Shrub |
| ***Pittosporum crassifolium*** | Shrub |
| ***Quercus ilex*** | Temperate Broadleaf Trees |
| ***Rhaphiolepis indica*** | Shrub |
| ***Rhus integrifolia*** | Shrub |
| ***Rhus ovata*** | Shrub |

| | |
|---|---|
| ***Schinus molle*** | Tropical Trees |
| **Species Name** | MEGAN PFT |
| ***Thevetia peruviana*** | Shrub |
| ***Ulmus parviflora*** | Temperate Broadleaf Trees |
| ***Westringia fruticosa*** | Shrub |
| ***Xylosma congestum*** | Shrub |

**Table 6.8.** Abundance of Species and their assigned PFT at 3 sites along SR-55

| Sampling Date | Species Name | Percent | PFT |
|---|---|---|---|
| **Site 1** | | | |
| **November** | *Quercus ilex* | 39 | Temperate Broadleaf Trees |
| **November** | *Schinus molle* | 1 | Tropical Trees |
| **November** | *Ulmus parviflora* | 0 | Temperate Broadleaf Trees |
| **November** | *Xylosma congestum* | 60 | Shrubs |
| **Site 2** | | | |
| **November** | *Quercus ilex* | 8 | Temperate Broadleaf Trees |
| **November** | *Schinus molle* | 20 | Tropical Trees |
| **November** | *Ulmus parviflora* | 2 | Temperate Broadleaf Trees |
| **November** | *Xylosma congestum* | 70 | Shrubs |
| | | | |

| Sampling Date | Species Name | Percent | PFT |
|---|---|---|---|
| **Site 3** | | | |
| **September** | *Quercus ilex* | 0 | Temperate Broadleaf Trees |
| **September** | *Schinus molle* | 55 | Tropical Trees |
| **September** | *Ulmus parviflora* | 5 | Temperate Broadleaf Trees |
| **September** | *Xylosma congestum* | 40 | Shrubs |

### 6.3.1 Input Structure

The VEM reads all required inputs from an Excel file consisting of three logical data groups:

1. **Config**

   Contains scalar and string parameters in a two-column format (Field, Value). These include vegetation and meteorological constants such as latitude, relative humidity (RH) and leaf area index (LAI) constants, atmospheric pressure, soil moisture at 10 cm, evapotranspiration coefficients, and several on/off switches for MEGAN stress algorithms.

2. **PFT**

   Lists species names and their relative cover percentage. The function automatically aggregates these species fractions into the six MEGAN Plant Functional Types (PFTs) and constructs a PFT fraction table required by the emission model.

3. **Meteorological**:

   Provides a time-resolved series of meteorological drivers such as timestamp, temperature, and wind speed. The model includes a timestamp parser capable of handling MATLAB datetimes, Excel serial dates, and mixed-format text strings.

For each timestep, additional meteorological drivers required by MEGAN (e.g., PPFD, LAI, RH/QV, atmospheric pressure) are assembled into a structured *Met* table.

### 6.3.2 Model Preprocessing

Before running MEGAN algorithms, the function performs several preprocessing tasks:

- Parses the timestamp column and enforce the appropriate time zone (Example: UTC, PST, HST, AKST, MST, CST, EST).
- Compute day-of-year, hour, PPFD, and other diagnostic variables.
- Build a parameter table containing RH, latitude, soil moisture, and several MEGAN gamma-factor switches (e.g., GAMHT, GAMLT, GAMAQ).
- Constructs the emission factor and light-dependent fraction (EF, LDF) table for all 19 species.
- Converts user-supplied species-level vegetation fractions into MEGAN's 6 PFT types.

### 6.3.3 Core Emission Computation

For each timestep, the model:

1. Compute canopy radiation, sunlit and shaded PPFD, leaf temperature, and stomatal resistance across five canopy layers using Gaussian quadrature.
2. Evaluates MEGAN environmental response factors:
    - $\gamma_t$ (temperature response),
    - $\gamma_P$ (light response),
    - γ_HT, γ_LT, γ_HW, γ_AQ, γ_$CO_2$,
    - γ_SM (soil moisture stress),
    - γ_LA, γ_BD, etc.
3. Combines these gamma factors with PFT specific emission factors (EF), LDF, leaf area index, and canopy distribution to compute hourly emissions for all 19 VOC species in **nmol $m^{-2}$ $s^{-1}$**.

4. Converts emissions to **mg $h^{-1}$** using species molecular weights and the modeled ground footprint area, producing physically interpretable emission rates.

### 6.3.4 Output Tables

Two output tables are produced:

1. **EmisTbl**
   Contains *Day*, *Hour*, and emission rates (mg $h^{-1}$) for all **19 MEGAN VOC species**. This table represents the complete biogenic emission inventory generated by the simplified VBM.

2. **IsopTbl**
   A reduced table focused on an investigator-selected "preferred species" (default: isoprene). In addition to the modeled emission rate, this table includes key meteorological drivers: temperature, PPFD, LAI, and soil moisture. This table is primarily used for comparison with observational datasets.

If the user specifies an output Excel filename, the function automatically writes:

- **All_Emissions** (full 19-species inventory)
- **Selected_Species** (reduced table)

Table 6.9 is the sample final result for November high porosity section (

Table 6.8 Site 2). The emission rates per unit area computed by MEGAN are converted to emission rates for the entire barrier using the product of the Leaf Area Index and the horizontal area covered by the vegetative barrier.

The results are expressed as **Emission Rates (mg/h).** Table 6.9 provides emission rates of 4 out of a total of 19 VOC species included in the model.

**Table 6.9.** *Example emission rate (mg/h) results for SR-55 Site 1 sampled in November (e.g., high porosity section). Only 4 of the 19 VOC species are listed for readability.*

| Day | Hour | isoprene | Pinenes | ocimenes | carene |
|---|---|---|---|---|---|
| **266** | 7 | 217.84 | 53.27 | 8.12 | 17.64 |
| **266** | 8 | 386.40 | 62.94 | 11.96 | 18.74 |
| **266** | 9 | 521.91 | 72.54 | 15.07 | 20.46 |
| **266** | 10 | 623.75 | 79.83 | 17.36 | 21.82 |
| **266** | 11 | 693.63 | 85.06 | 18.92 | 22.87 |
| **266** | 12 | 685.30 | 83.67 | 18.72 | 22.40 |
| **266** | 13 | 686.01 | 84.14 | 18.73 | 22.61 |
| **266** | 14 | 670.30 | 84.47 | 18.42 | 23.05 |
| **266** | 15 | 672.43 | 88.90 | 18.59 | 24.97 |
| **266** | 16 | 571.88 | 86.29 | 16.54 | 25.56 |
| **266** | 17 | 320.91 | 73.21 | 11.21 | 24.20 |

.

## 6.3.5 Summary

The Vegetative Barrier Model (VBM) integrates two linked components—a **Dispersion Model (DM)** and a **VOC Emission Model (VEM)**—to evaluate the dual role of roadside vegetation in modifying pollutant concentrations and generating biogenic emissions. The DM, formulated in earlier chapters, uses line-source geometry, receptor locations, vegetation characteristics, emission rates, and hourly meteorological fields (from AERMET .sfc files) to estimate $PM_{10}$ concentrations downwind of a highway. Inputs include roadway dimensions, barrier properties such as height, porosity, and leaf area index, traffic-based emission factors, and turbulence parameters derived from .sfc variables such as friction velocity and Monin–Obukhov length. The model outputs concentration time series at user-specified receptors.

The VEM is based on the MEGAN2.1 framework and estimates emissions of 19 VOC species from the vegetative barrier. Plant species observed at barrier sites are mapped to MEGAN Plant

Functional Types (PFTs), allowing the model to compute PFT-weighted emission factors. The VEM reads three input groups—configuration parameters, species fractions, and meteorological time series—and performs preprocessing to construct canopy radiation, PPFD, environmental response factors, and MEGAN gamma-factor modifiers. For each hour, it calculates VOC emission rates, converts them to mg $h^{-1}$ using molecular weights and barrier footprint, and outputs both full-species inventories and species-specific tables (e.g., isoprene).

The Dispersion Model (DM) and the VOC Emission Model (VEM) form an integrated Vegetative Barrier Model (VBM) for assessing how vegetative barriers modify near-road PM concentrations while simultaneously generating VOC emissions that can influence secondary pollutant formation. The VBM is implemented in MATLAB and has been compiled into an executable with a user-friendly interface, allowing non-experts to apply the model with minimal effort.

## 6.4 References


- Guenther, A. B., Jiang, X., Heald, C. L., Sakulyanontvittaya, T., Duhl, T., Emmons, L. K., and Wang, X. (2012). *The Model of Emissions of Gases and Aerosols from Nature version 2.1 (MEGAN2.1): An extended and updated framework for estimating biogenic emissions*. Geoscientific Model Development, 5, 1471–1502.